1981

An assessment of the blue route bridge electroslag weldments, December 1981

J. W. Fisher

A. W. Pense

J. D. Wood

B. T. Yen

Lehigh University

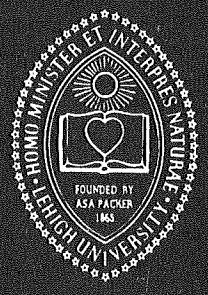

Study of Blue Route Bridge

Defects and Structural Response

AN ASSESSMENT OF THE BLUE ROUTE BRIDGE ELECTROSLAG WELDMENTS

by
John W. Fisher
Alan W. Pense
John D. Wood
Ben T. Yen
Rajan Dias
John Edinger

Fritz Engineering Laboratory

December 1981
Report No. 457-1 (81)

COMMONWEALTH OF PENNSYLVANIA

Department of Transportation

Research Division

Wade L. Gramling - Chief Research Engineer
Istvan Janauschek - Research Coordinator

Study of Blue Route Bridge Defects and Structural Response

AN ASSESSMENT OF THE BLUE ROUTE BRIDGE ELECTROSLAG WELDMENTS

by
John W. Fisher
Alan W. Pense
John D. Wood
Ben T. Yen
Rajan Dias
John A. Edinger

Prepared in cooperation with the Pennsylvania Department of Transportation and the U. S. Department of Transportation, Federal Highway Administration.

LEHIGH UNIVERSITY

Office of Research

Bethlehem, Pennsylvania

December 1981

Fritz Engineering Laboratory Report No. 457-1(81)

TABLE OF CONTENTS

		Page
	ABSTRACT	iii
1.	INTRODUCTION	1
2.	STRESS HISTORY STUDY	3
3.	MATHEMATICAL MODEL	6
4.	THERMAL STRESSES	7
5.	MATERIAL PROPERTIES	10
	5.1 Fracture Toughness of Weld Metal	11
	5.2 Chemistry	12
6.	METALLOGRAPHIC STUDIES	13
7.	ANALYSIS AND EVALUATION OF DEFECTS	15
8.	CONCLUSIONS AND RECOMMENDATIONS	16
	TABLES	17
	FIGURES	25
	REFERENCES	62
	ACKNOWLEDGMENTS	63

ABSTRACT

Live load stresses, thermal stresses, and the temperature gradients were measured on two of the main longitudinal girders of the Blue Route Bridge on I-476 over the Schuylkill River. Core samples were removed from several electroslag welds that contained discontinuities and were examined in order to assess the defects and correlate the defects with the non-destructive tests. The fracture toughness characteristics of the weldment were also determined.

The measured live load stresses indicated that full composite action existed between the concrete deck and the main girders. The live load stresses measured in the top flange electroslag welds were always less than 0.5 ksi under all loading conditions. The thermal gradient was recorded at several sections. The temperature gradient was used to compute stresses, in the top flange, which were found to be about 1.5 ksi at the most severe thermal conditions.

Destructive examination of the weld core samples revealed that the defects were not critical. The fracture toughness of the embedded top flange electroslag weldments was found to be adequate, and no retrofitting of the welds is considered necessary.

1. INTRODUCTION

The Blue Route Bridge over the Schuylkill River is part of I-476 which passes through Conshohocken, PA. Figure 1 shows the plan and elevation of the twin bridge structures that carry the northbound and southbound traffic over the Schuylkill River. Details of the framing plan for the main river spans are given in Fig. 2. Figure 3 shows a view along one of the main longitudinal girders of the southbound span. The cross section of these structures is given in Fig. 4. The main longitudinal girders have transverse floor beams supporting six longitudinal stringers. The Blue Route bridge was one of three bridges in the state that was examined because it contained electroslag groove welds in the main girder flanges.[1] This examination demonstrated that the electroslag groove welds had low levels of notch toughness and flaws were detected in a number of the weldments. Several of the electroslag groove welds in bottom tension flanges required splicing. A nondestructive examination of the top flange groove welds was carried out with ultrasonic probes. No significant discontinuities were observed in the portions of the top flange welds that were examined. As a result of this finding, none of the top flange tension welds which were embedded in the concrete slab were spliced. To reduce the influence of tensile residual stresses at the web-flange fillet welds, slotted holes were placed in the web directly below the top flange electroslag welds. One of these slots is shown in Fig. 5.

One of the objectives of this study was to examine the cyclic stress conditions that occurred at these embedded groove welds. Since the structure was designed as a non-composite system, it was desirable to confirm its actual behavior and establish whether or not undetected

discontinuities might be susceptible to crack propagation. Studies on a similar structure had demonstrated that some degree of composite behavior was likely.

2. STRESS HISTORY STUDY

During September 1979, 46 strain gages and 10 temperature gages were installed at five cross sections and at electroslag weldments at locations identified in Fig. 6. Four of the cross sections were located on downstream girder G8 of the northbound bridge. The fifth cross section was located on up stream girder G7. In addition, gages were also installed at several of the electroslag groove welds of Girders G7 and G8 as shown schematically in Fig. 6b.

Strain gages and temperature gages were installed at several locations on a cross section as illustrated in Fig. 7. This depicts the gage location for cross section 2 which was 14 ft. west of pier 7. Figure 8 show the gages and wiring attached to the downstream girder near pier 7.

The gages were connected to cables which hung from the bridge to the river bank below, where the FHWA instrumentation trailer was located. The 46 strain gages were connected to amplifiers and recording units. Both analog oscillograph records and digital data were obtained.

Strain measurements were recorded on September 26 and 27, 1979. Altogether, records for 212 trucks crossing the bridge were obtained. Several records included the effect of more than one truck on the bridge.

Temperature readings were taken at intervals of half an hour commencing at 7:30 AM on September 26 and extending to 8:30 AM on September 28.

A test truck of known weight and axle load distribution is shown in Fig. 9. The test truck made 12 runs across the bridge as summarized

in Table 1. Speed and lane records were obtained in order to assess the dynamic response and provide a reference condition for further studies.

From the recorded analog and digital records, the stress range excursions under the random truck traffic loading was determined. The test data were recorded throughout the test period. Stress histograms were developed for each gage location at the five sections and at electroslag welds.

As expected, the stress distribution at each girder cross section was not symmetric over the negative moment zone adjacent to pier 7 or in the positive moment region in spans 7 and 8. Figures 10 to 13 show the measured strain gradients for the four cross sections of girder G8 during test truck run 10. Also plotted in Figs. 10 to 13 is the theoretical strain gradient for a fully composite section as well as the gradient for noncomposite behavior at the design stress. It is apparent that the neutral axis under live load is near the top flange at all cross sections. Hence, the structure was responding to the live load as a "composite" structure even though the slab was not attached with shear connectors.

The maximum recorded stress range due to traffic was 3.0 ksi in the positive moment region of spans 7 and 8 at cross sections 1 and 4. The maximum stress range recorded in the top tension flange at pier 7 was 0.45 ksi (section 3). At the electroslag welds located near sections 2 and 3, the recorded stress range at the top tension welds were nearly zero as can be seen in Figs. 11 and 12. Figure 14 shows a typical strain-time response as recorded by analog recorder during passage of the test track. It can be seen that very little change in stress occurs in the embedded top tension flange.

In order to assess the effect of cyclic stresses, the stress range occurrences were plotted as histograms. The stress range occurrence data for the bottom flange of the positive moment regions are shown in Figs. 15 and 16 for span 7 (cross section 1) and span 8 (cross section 4). Both plots show the characteristic skewed stress range distribution observed in most bridge structures.

Figure 17 shows the compression stress range spectrum observed in the bottom flange at cross section 3. This section was 2.5 ft. east of pier 7. Its shape is similar to that observed at sections 1 and 4.

The embedded top flange at the east groove weld from pier 7 in girder G7 only provided 10 occurrences at a stress range between 0.35 and 0.55 ksi. Most of the other instrumented electroslag groove welds (see Fig. 6b) had even lower stress range occurrences. Hence all electroslag weldments embedded in the flange experienced negligible stress cycles. This can also be seen in Fig. 14 where strain measurements at all of the electroslag weldments were negligible during the test truck passage at 51 mph.

3. MATHEMATICAL MODEL

In order to simulate mathematically the behavior of the bridge and to evaluate the effects of nonuniform thermal distribution on the cross section, a finite element analysis of the structure was carried out.

Figure 18 shows the finite element model of the six-span structure. Also shown is the cross section of the main girders. Four plane stress elements (elements 4, 5, 6 and 7) were used to model the main girder webs. The flanges (elements 3 and 8) were modeled with truss elements. The slab (element 1) was modeled with a three dimensional beam element and a truss element since the computed program makes no allowance for temperature input into the beam elements. The slab to flange connection (element 2) consisted of a vertical beam element with a high flexural inertia in order to simulate composite behavior.

The behavior of the bridge under live load showed that the computer model accurately represented the bridge. The stress distribution measured in the field was in accord with the predicted distribution as can be seen in Figs. 10 to 13.

Table 2 compares the location of the neutral axis predicted by the theoretical finite element analysis and measured location for four different load cases. It is apparent from Table 2 and Figs. 10 to 13 that a fully composite section exists throughout the structure.

4. THERMAL STRESSES

Thermal gradients over sections of multispan continuous girder bridges create stresses in the girders that equal or exceed the stresses due to traffic.[2]

Temperature in various parts of a bridge differ from the air temperature. The daily bridge component temperature variation depends upon the material, the location of the component in the bridge, the configuration of the bridge, and the bridge's orientation with respect to the sun and wind. Differences in the component temperature will result in a nonlinear temperature and stress distribution. A finite element analysis was carried out in order to evaluate the influence of the observed thermal conditions in the Blue Route Bridge.

The predicted stress variation over the cross section of the main girders was evaluated for temperature conditions that simulated the field observations so that comparisons with the field measured stress data could be made. In addition the maximum stresses were estimated that corresponded to the variation between a hot day and a cold night.

The temperature gages at the locations shown in Figs. 6a and 7 were read during the period between September 26 and September 28, 1979.

Temperature versus time relationships were obtained for three cross sections. All exhibited similar characteristics. Approximately 75% of the web of girder G8 was exposed to the sun during the morning and noon hours. Figure 19 shows the variation observed in cross section 1 of the south girder (G8) at the three gage locations during the measurement period which commenced at 0750 on September 26, 1979. As illustrated

in Fig. 19 a significant differential temperature distribution resulted between the temperature gages installed on the girder web and bottom flange and the gage installed on the embedded top flange. The temperature differential is the difference from the 0750 first day temperature which was used as a reference point. Table 3 provides a tabulation of the values plotted in Fig. 19 for cross section 1.

The average values tabluated in Table 4 for the applicable cross sections were input into the finite element model. Figure 20 shows the thermal gradients that were assumed at cross section 1 for three intervals of time. Emanuel and Hulsey[3] suggest that the temperature distribution does not vary linearly with depth, but is nearly constant throughout the web depth and then abruptly changes to the slab temperature at the top flange.

The computed thermal stress distribution at several girder cross sections are plotted in Fig. 21 for a "hot" day. The stresses can be seen to increase from the end of the bridge and reaches maximum over pier 7. The steel girders develop a tensile thermal stress in the top flange and concrete deck, and compression thermal stresses in most of the web and bottom flange. The thermal stress gradients were nonlinear at all five sections that are plotted in Fig. 21. The computed maximum thermal tensile stress was 1.4 ksi in the top flange at the support and at the electroslag flange welds. The maximum compression thermal stress occurred in the lower web and bottom flange and was equal to 4.8 ksi. The computed thermal tensile stress in the concrete slab over pier 7 was 140 psi.

As the temperature is decreased during the night, the steel beam cools more rapidly than the slab and the top flange and the cold night

distribution shown in Fig. 22 results. As expected, this reversed the stress components and placed the embedded top flange into compression and most of the web and bottom flange into tension. The maximum compression thermal stress was 0.8 ksi at pier 7 and the adjacent electroslag weldments. The bottom flange tensile thermal stress reached 2.8 ksi.

The thermal stress cycle which develops daily would appear to be the highest stress cycle that the electroslag weldments will experience. However, the thermal stresses are relatively small and will occur at most once a day.

5. MATERIAL PROPERTIES

A preliminary examination of three electroslag weld metal cores removed from the Blue Route Bridge was provided in Ref. 1. Three 3 in. diameter cores were removed from the bridge structure and sliced into segments. Charpy V-notch tests were carried out on these samples and resulted in average values of 5 ft-lbs for core G5K and 4.3 ft-lbs for core G6D at 0^{o}F. The results of these tests are summarized in Table 5. The third core (G2D) had considerable variation in absorbed energy as can be seen from the tabulated values.

Three additional cores, 4 in. in diameter were removed from the Blue Route Bridge when retrofit splices were installed. These cores were centered over defects in the weldments in order to permit a destructive examination of the defects and additional material tests where enough sound weldment was available.

These cores were located at the points described hereafter.

Core G1E - Span 6, North Girder of the southbound bridge, weld 2, first joint south of pier 6. See Fig. 23.

Core G6A - Span 7, South Girder of the southbound bridge, weld 1, first joint north of pier 6. See Fig. 24.

Core G7A - Span 11, North Girder of the northbound bridge, weld 3, first joint south of pier 11. See Fig. 25.

Cores G1E and G6A were removed from electroslag welded joints while Core G7A was removed from a multipass submerged arc welded joint. Cores G1E and G6A were located with their edges 3 in. from the flange tip; Core G7A was located with its edge 3.5 in. from the flange tip.

5.1 Fracture Toughness of Weld Metal

Cores G1E, G6A and G7A were sliced at the location of the weld defects as indicated by the nondestructive tests. Metallographic studies were carried out on each slice prior to fabricating additional Charpy V-notch specimens. The results of the metallographic studies are discussed in Chapter 6.

The Charpy V-notch specimens were all notched at the centerline of the welds. The results of these additional tests are summarized in Table 6. All of the Charpy V-notch tests summarized in Tables 5 and 6 are plotted in Fig. 26. It is readily apparent that the electroslag weldments had much lower levels of absorbed energy than the the multiple pass submerged arc weld. The electroslag welds exhibited more scatter in the test data.

The Charpy V-notch test data was transformed into dynamic fracture toughness values using Barsom's correlation equation.

$$K_{Id} = (5\ E\ CVN)^{1/2} \qquad (1)$$

The results of this transformation are plotted in Fig. 27 for the electroslag welds. The test points are compared with the range of fracture toughness reported in Refs. 4 and 5 for dynamic and static loading.

The results of the tests on Cores G5K and G6D indicate low fracture toughness at $0^{o}F$. Only two CVN tests were conducted on Core G1E at $0^{o}F$, with one high and one low value of absorbed energy being obtained. All tests on Core G6A were performed at $40^{o}F$. The electroslag weldments showed lower absorbed energy values than the submerged arc weldment as is evident in Fig. 26. The wide scatter in the data can be attributed to the variation in grain size and grain orientation with respect to the notch.

Two 1 in. thick compact tension tests were carried out on specimens fabricated from electroslag weld Cores G1E and G6A. Both tests were carried out at -30° F at a 1 sec. loading rate. Figure 28 shows the load-deflection curve for the specimen from core G6A. The K_c values obtained for 1 second loading rate were low, with values of 44.3 and 44 ksi $\sqrt{in.}$ for Cores G1E and G6A, respectively. These results are shown in Fig. 27 as the open dots. It can be seen that the 1 sec. loading rate level of fracture resistance is about equal to the upper bound dynamic fracture toughness at -30° F.

The Charpy V-notch data from submerged arc weld Core G7A are plotted in Fig. 29. It is apparent that the dynamic fracture toughness is near the upper bound of the electroslag weld scatter band.

5.2 Chemistry

A weld metal chemical analysis check was carried out on parts of broken Charpy V-notch specimens or the compact tension specimens from Cores C1E and G6A. The results are summarized in Table 7 and reveal no major irregularities. The results are directly comparable with the weld metal chemistry found in Cores G5K, G6D and G2D.[1]

6. METALLOGRAPHIC STUDIES

The three flange core samples G2D, G5K and G6D were each cut into segments after the exterior surfaces of the cores were polished and etched. Cores G2D and G5K were sliced to obtain two 10 mm thick slices. Core G6D was sliced so that three 10 mm slices were available. Each of these slices was polished and etched in order to examine the weld microstructure and detect any grain boundary fissures. No evidence of grain boundary fissures were detected in cores G2D, G5K or G6D.[1]

The photomicrographs for cores G2D, G5K and G6D are given in Ref. 1. These show the large grain structure of the electroslag weldments as well as extensive evidence of repair weld along the fusion line.

Cores G1E, G6A and G7A were also polished and etched to reveal the welds. The electroslag weldment from G1E (see Fig. 23) had substantial repair welds along the fusion lines as can be seen in Fig. 30. Figure 31 shows the multipass submerged arc weldment G7A with a repair weld near one end. Figure 32 shows the electroslag weldment from G6A. No defects were detected on the surfaces of any of these weldments.

Table 7 provides a summary of the nondestructive test results reported at the location of each core. The weldment defects indicated by the ultrasonic and radiographic tests were used to develop destructive cutting schemes. These are shown in Figs. 33 to 35. Each of the slice segments was polished and etched in order to examine and identify the type and location of any defect.

A slice near the weld defect which was indicated to exist in core G1E did not reveal any major defect as can be seen from the polished and etched

surface shown in Fig. 36. The photomicrograph shows several repair welds at the fusion line.

The fusion line region was examined at 50X at the weld repair region. This is shown in Fig. 37. The photomicrograph shows a dispersion of nonmetallic inclusions near the fusion line. Apparently the large number of these small discontinuities were responsible for the +9Db ultrasonic test rating indicated to exist at this location. No other discontinuities were observed on any of the other polished and etched surfaces.

Figure 38 shows the polished and etched segment of core G6A near the indicated defect. The microstructure of the electroslag weldment is readily apparent. The defect can be seen near the center of the weldment in Fig. 38. It was identified as a slag inclusion about 1 mm (0.04 in) in diameter. Figure 39 shows a photomicrograph at 40X of the slag inclusion which has a circular shape on the sawcut plane. The large grain structure of the electroslag weld is apparent in both Figs. 38 and 39.

Figure 40 shows the polished and etched edge of the sawcut of the submerged arc weld in core G7A. No significant defect was apparent on the surface except a small slag inclusion on the fusion line. Figure 41 shows a photomicrograph at 50X of the slag inclusion. It can be seen that a spherical shaped piece of slag was trapped on the fusion line.

The destructive examination of cores removed from the Blue Route Bridge has indicated that all of the indicated defects were very small. None of the defects appeared to be significant.

7. ANALYSIS AND EVALUATION OF DEFECTS

The destructive examination of cores removed from weldments with indicated defects has shown that all of the defects were very small spherical like discontinuities. All defects were embedded in the weldments or along the fusion line. The stress intensity factor for such defects is bounded by the relationship

$$\frac{2}{\pi}\sigma\sqrt{\pi a_1} \leq K \leq \sigma\sqrt{\pi a_2} \qquad (2)$$

where a_1 is the radius of the circular shaped planar crack and a_2 the half width of an elongated defect.

None of the flaws detected in the Blue Route Bridge would likely result in fracture unless they were enlarged by fatigue crack growth.

The largest detected defect had a radius of 0.02 in. Both of the relationships provided by Eq. 2 would generate stress intensity ranges ΔK well below the crack growth threshold of 2.6 ksi $\sqrt{in}$ observed with the Meadville crack growth specimens. As illustrated in Section 2, the maximum stress range in the bottom flange was 3 ksi. This yields a maximum stress intensity range of 0.75 ksi $\sqrt{in}$. Even the design stress range would result in ΔK values below the crack growth threshold.

Since the embedded top flange experiences even smaller values of stress range (0.45 ksi), no crack propagation will ever develop in the embedded top flanges of the Blue Route Bridge.

No crack instability should develop in any of the top flange weldments.

8. CONCLUSIONS AND RECOMMENDATIONS

(1) The results of the stress history and thermal stress studies carried out on the Blue Route Bridge has demonstrated that the embedded top flanges act compositely with the concrete slab under live load. As a result negligible stress cycles are experienced by the electroslag weldments in the top flanges.

(2) The highest stress cycle experienced by the flanges of the longitudinal girders occurs as a result of the thermal stress introduced by temperature gradients on the cross section. The stress range in the embedded flange due to the thermal gradient do not exceed 1.5 ksi, and is at most a daily stress cycle.

(3) The destructive examination of the weld core samples that contained rejectable defects demonstrated that all of the defects were not critical. None would result in fatigue crack growth and all had ample margins of safety against fracture.

(4) The measured fracture toughness of the electroslag weldments at $-30^{o}F$ was found to be 44 ksi $\sqrt{in}$ at 1 sec. loading rate. This placed the fracture resistance of the electroslag weldments near the upper bound of the dynamic fracture toughness bond.

(5) The study has shown that no further retrofitting is needed for the Blue Route electroslag weldments. All embedded top tension flange welds will provide satisfactory service.

(6) It is recommended that the top flange electroslag tension welds be nondestructively tested if the slab is ever removed for replacement.

Table 1 Test Truck Run Data

Run No.	Time (PM)	Lane	Speed (mph)
1	1:04	Curb 1	17
2	1:16	Middle 2	9
3	1:35	Passing 3	9
4	1:50	Curb 1	8
5	2:03	Middle 2	7
6	2:12	Passing 3	8
7	2:28	Curb 1	51
8	2:38	Middle 2	52
9	2:48	Passing 3	46
10	3:01	Curb 1	51
11	3:14	Middle 2	52
12	3:25	Passing 3	52

Table 2 Location of Neutral Axis X-Sections 1 & 2

Case		Condition	Distance above Bottom Flange
Design		Non-Composite	78 (in.)
Measured	X-Section 1	Test Truck Run 1	60
	1	4	60
	1	7	56
	1	10	53
	2	1	46
	2	4	51
	2	10	47
FE		Fully Composite	55

Table 3 Temperature vs Time
Cross Section 1

Time (hr)	Temperature Difference (^{o}F) Top	Middle	Bottom
7.50	0.0	0.0	0.0
8.50	-1.0	1.3	-0.5
9.00	-0.8	4.8	7.0
9.50	-0.5	8.1	10.7
10.50	0.8	15.3	19.4
11.50	2.0	22.5	28.3
12.00	2.4	26.8	32.8
12.50	3.8	32.5	36.5
13.50	5.1	33.4	32.3
14.50	6.4	32.7	27.2
15.00	7.2	30.5	25.4
15.50	7.7	28.6	23.7
16.00	8.4	27.5	23.2
16.50	8.9	26.4	22.0
17.00	9.3	25.2	21.0
32.00	2.4	2.9	0.4
32.50	2.3	3.7	1.9
33.00	2.5	5.5	5.1
33.50	2.5	10.4	15.5
34.00	2.6	13.0	17.5
34.50	3.0	14.8	17.8
35.00	3.5	15.9	17.4
35.50	3.4	18.5	20.3
36.00	4.4	24.8	28.7
36.75	5.7	30.5	31.9
37.00	6.5	32.1	32.7
37.50	7.0	32.9	31.7
38.00	7.6	31.8	28.0
38.50	8.0	30.5	25.7
39.00	8.3	28.7	23.9
39.50	8.8	26.8	22.0
40.00	9.3	25.4	20.5
40.50	9.7	23.8	18.8
41.00	10.1	22.5	17.6
41.50	10.2	21.2	16.7
42.00	10.4	19.3	14.8
42.50	10.4	17.3	12.3
43.00	10.4	16.3	10.9
43.50	10.3	14.8	9.4
44.00	9.9	13.2	8.0
44.50	9.8	13.5	7.2
45.00	9.1	11.4	6.7
45.50	9.5	10.0	5.5
46.00	9.4	10.1	5.4
46.50	8.9	9.4	5.3
47.00	8.3	8.9	4.8
53.67	4.6	6.3	3.2
54.00	4.6	6.3	3.7
54.50	4.2	6.4	3.3
55.00	4.1	6.3	3.9
55.50	3.9	6.7	4.0
56.00	4.0	7.3	4.7
56.50	3.8	8.0	5.7

Table 4 Maximum Temperature Differential (^{o}F)

Cross Section	Top Flange	Web	Bottom Flange
1	5.1	33.4	32.3
2	3.1	27.3	30.0
3	3.2	28.7	26.1
Average	3.8	29.8	29.5

Table 5. Charpy V-Notch Test Data for Blue Route Bridge

Specimen	Type Flange	Absorbed Energy (ft-lbs.)	Lateral Expansion (mils)
G5K1-1	Tension	3.5	7.0
G5K1-2	"	4.5	8.5
G5K1-3	"	4.5	10.0
G5K2-1	"	6.0	4.0
G5K2-2	"	7.0	5.0
G2D1-1	Compression	8.5	15.5
G2D1-2	"	22.5	28.5
G2D1-3	"	5.0	12.0
G2D1-4	"	27.5	36.0
G2D2-1	"	15.0	9.0
G2D2-2	"	5.0	4.0
G2D2-3	"	34.0	16.0
G6D1-1	Compression	4.0	9.5
G6D1-2	"	5.0	10.0
G6D1-3	"	6.0	10.5
G6D2-1	"	3.5	8.0
G6D2-2	"	3.5	8.0
G6D2-3	"	3.5	8.0
G6D3-1*	"	22.0	10.0
G6D3-2*	"	18.0	13.0

*Tested at 38^{o}, all other specimens tested at $0^{o}F$

Table 6 Charpy V-Notch Test Data for Blue Route

Specimen	Test Temp. (^{o}F)	Absorbed Energy (ft-lbs)	Lateral Expansion (mils)	K_{ID} (ksi $\sqrt{in}$)
(A) Electroslag Welds				
G6A-1	40	15.0	10.5	47.43
G6A-2	40	8.0	4.5	34.64
G6A-3	40	10.0	6.0	38.73
G6A-4	40	24.0	15.0	60.0
G1E-1	0	4.0	2.5	24.5
G1E-2	0	16.0	9.0	48.99
(B) Multiple Pass Submerged Arc				
G7A-1	-30	15.0	6.0	47.43
G7A-2	-30	14.0	6.0	45.83
G7A-3	0	22.0	8.0	57.45
G7A-4	0	19.5	6.0	54.08
G7A-5	0	17.0	7.0	50.5
G7A-6	40	18.0	7.0	51.96
G7A-7	40	21.5	6.5	56.79
G7A-8	40	37.0	17.0	74.5
G7A-9	70	44.0	20.0	81.24
G7A-10	70	40.5	17.5	77.94

Table 7 Weld Metal Chemistry of Blue Route Weldments

	G1E	G6A
Carbon	0.17	0.13
Silicon	0.09	0.19
Manganese	0.79	1.04
Phosphorous	0.010	0.011
Sulfur	0.026	0.019
Chromium	0.059	0.347
Copper	0.037	0.175
Molybdenum	<0.01	<0.01
Vanadium	<0.01	<0.01
Nickel	0.02	0.175
Aluminum	<0.01	<0.01

Table 8 Summary of Nondestructive Testing

	Specimen	Type of Weld	Ultrasonic Test Rating	Radiographic Examination	Rating of Defect
1	southbound, span 7, girder G6A weld 1	Electroslag	-	minor gas holes indicated	Rejectable
2	southbound, span 6, girder G1E weld 2	Electroslag	+9	no defect indicated	Acceptable
3	northbound, span 11, girder G7A weld 3	Multipass Submerged Arc	+1	no defect indicated	Rejectable

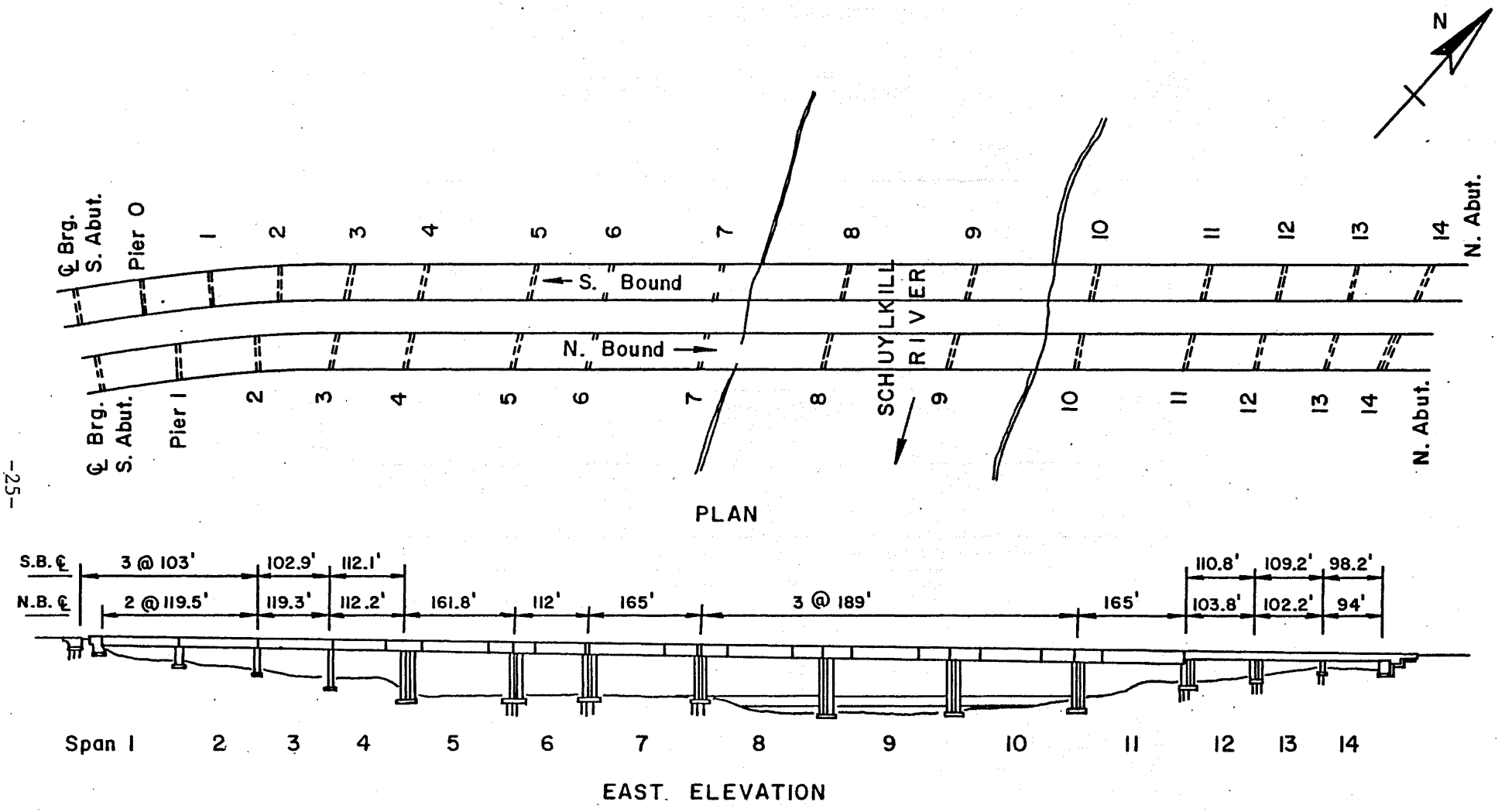

Fig. 1 Plan and Elevation of Blue Route Bridge

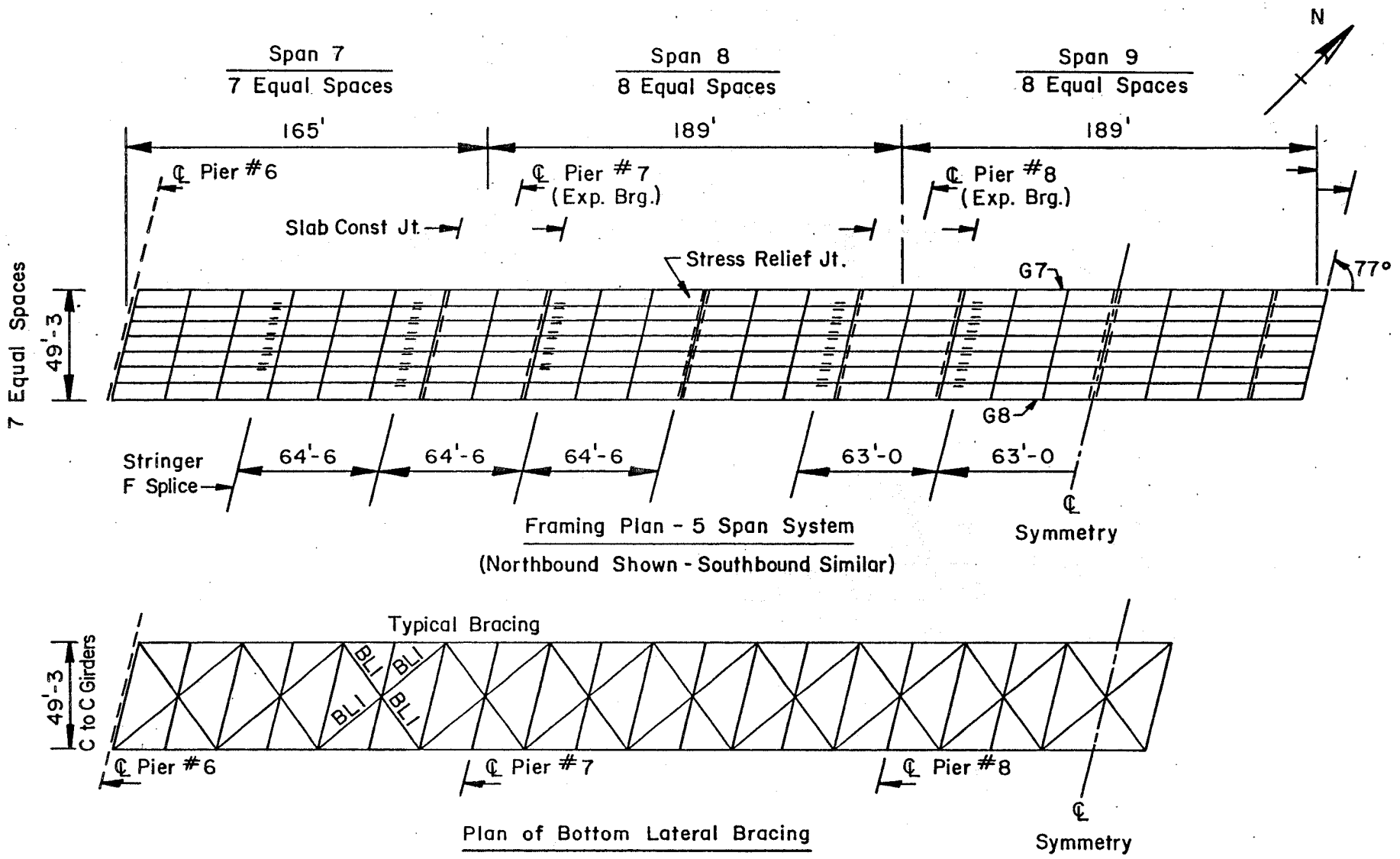

Fig. 2 Framing Plan for Main Girder Spans

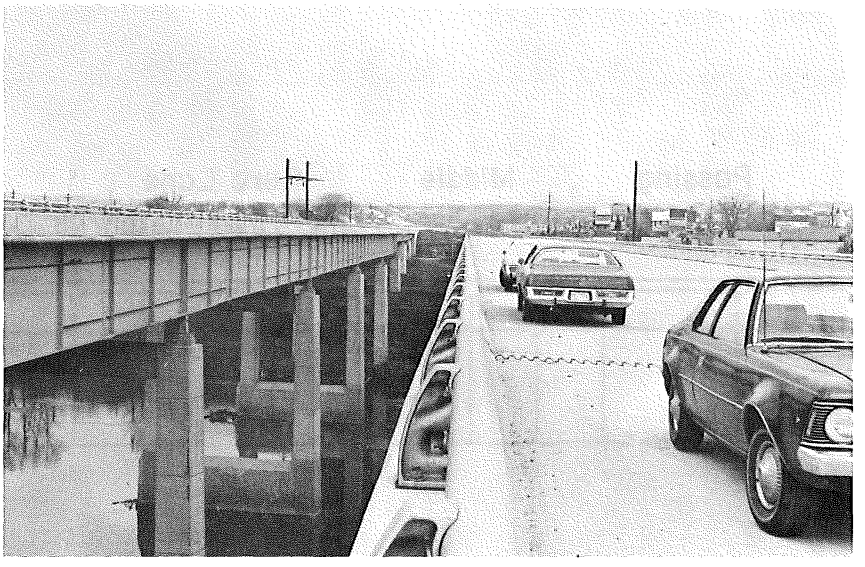

Fig. 3 Blue Route Bridge
(Looking North along Girder G7)

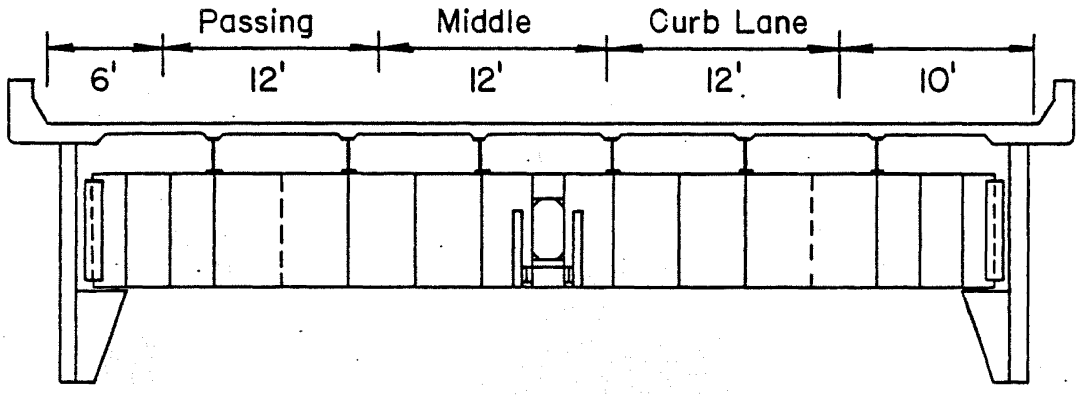

Fig. 4 Typical Cross-Section and Traffic Lanes

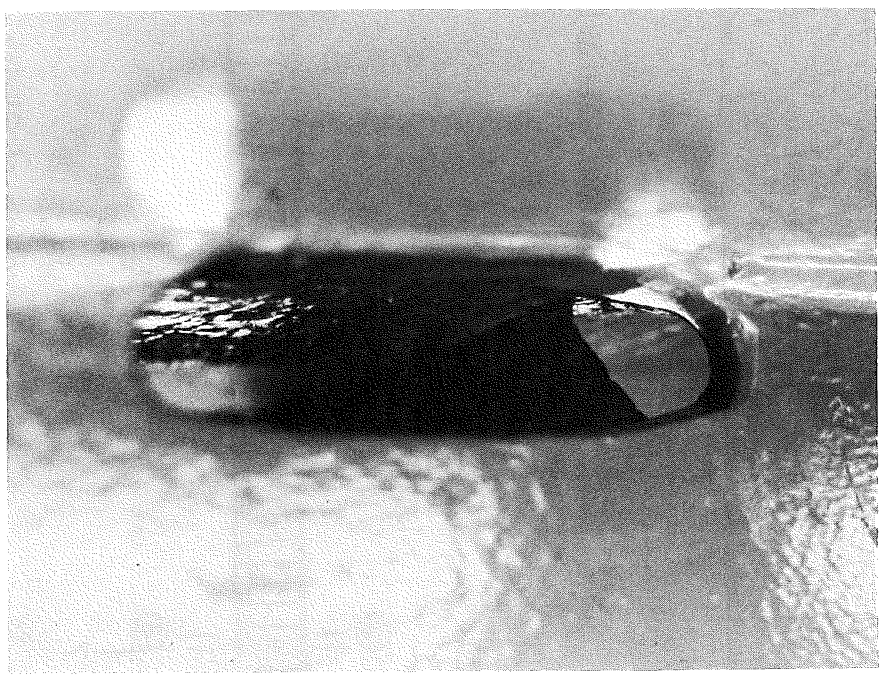

Fig. 5 Web Slot below Top Flange Electroslag Weld

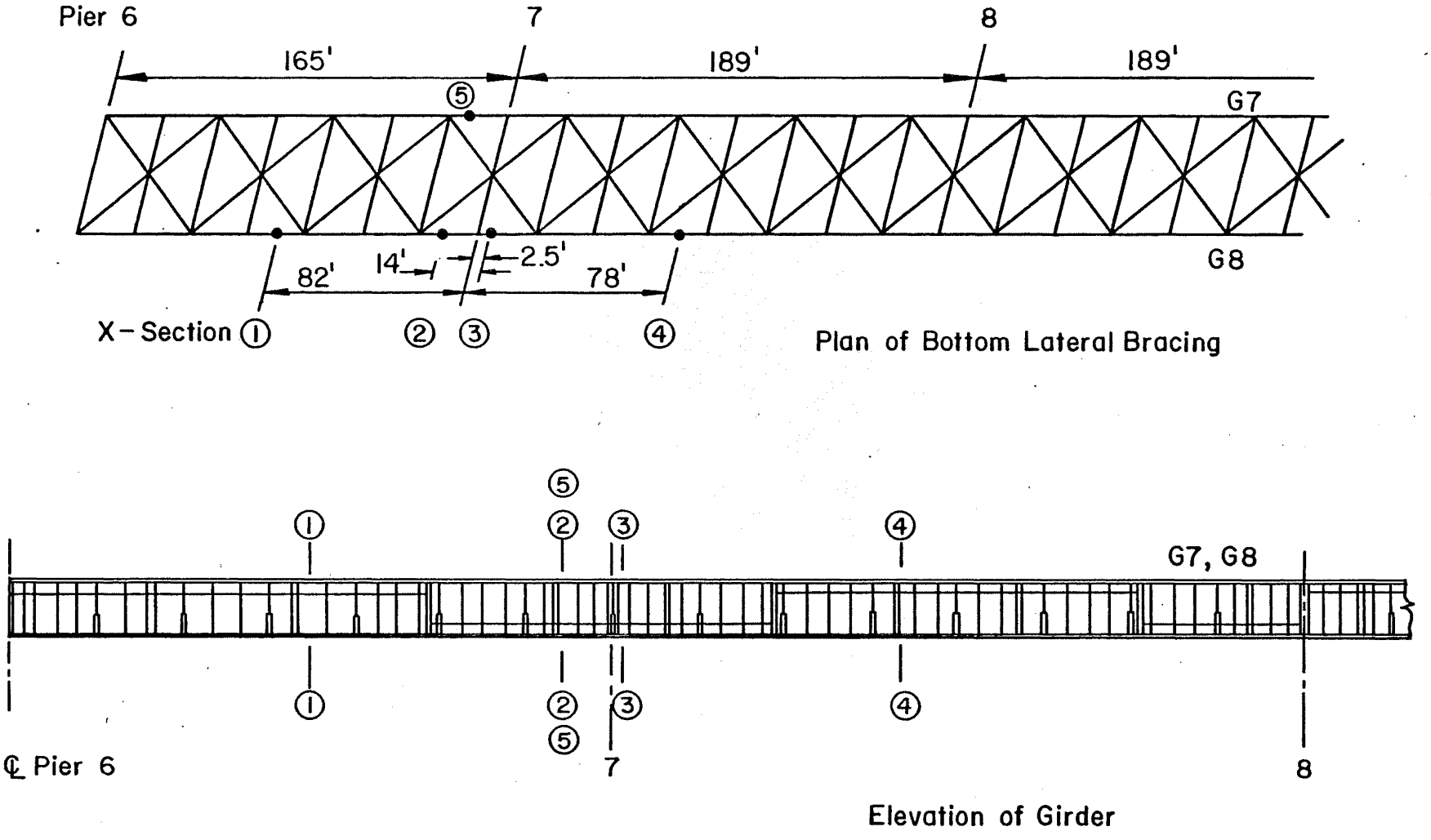

Fig. 6a Location of Gage Cross-Sections

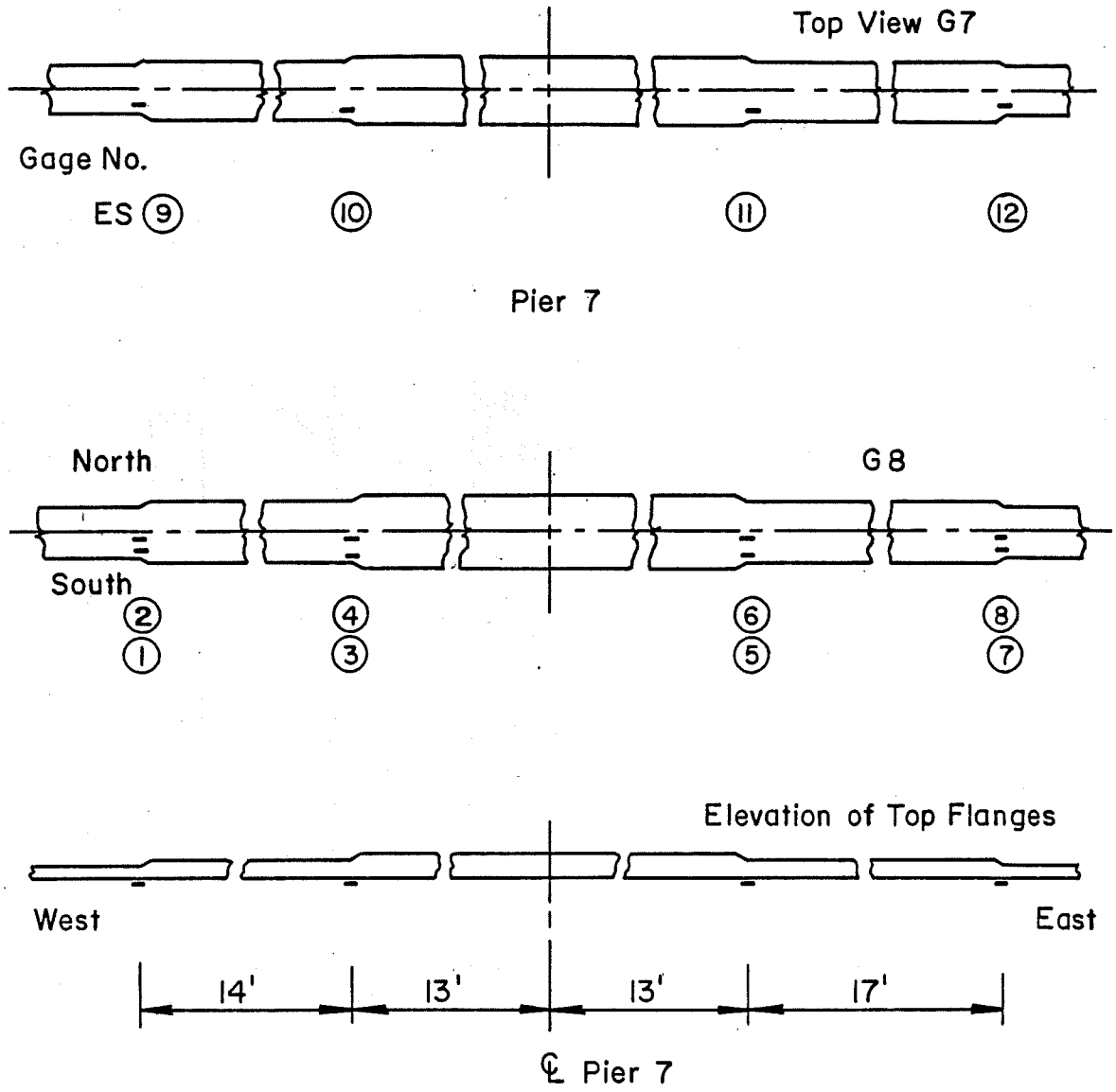

Fig. 6b Location of Strain Gages at Top Flange Electroslag Welds

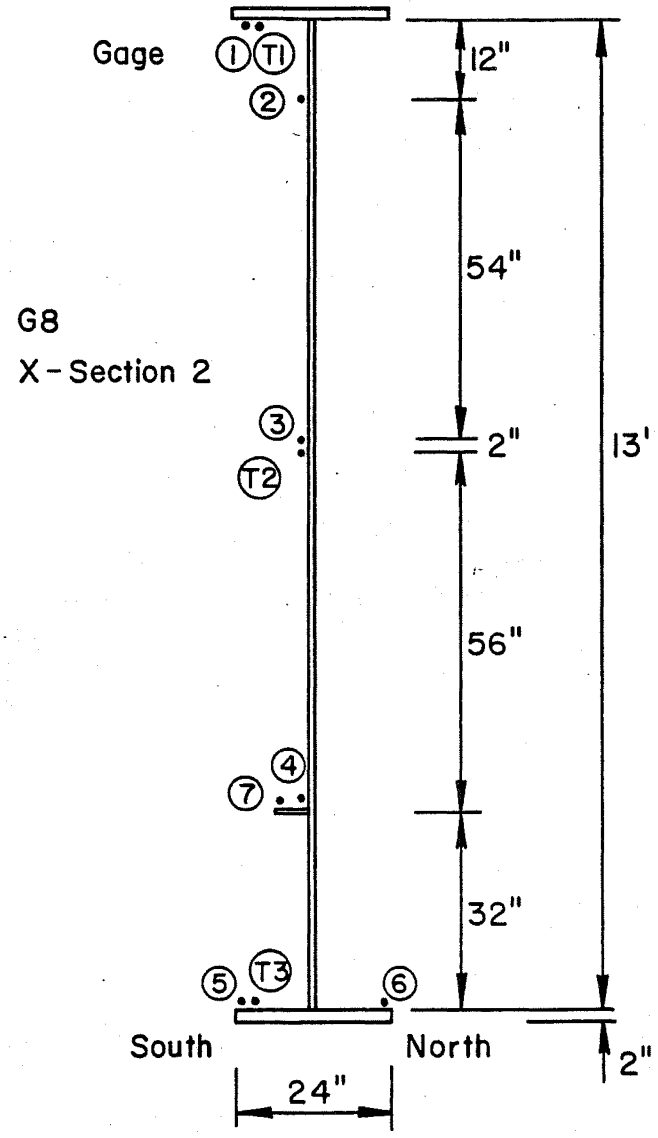

Fig. 7 Location of Strain and Temperature Gages, Cross-Section 2

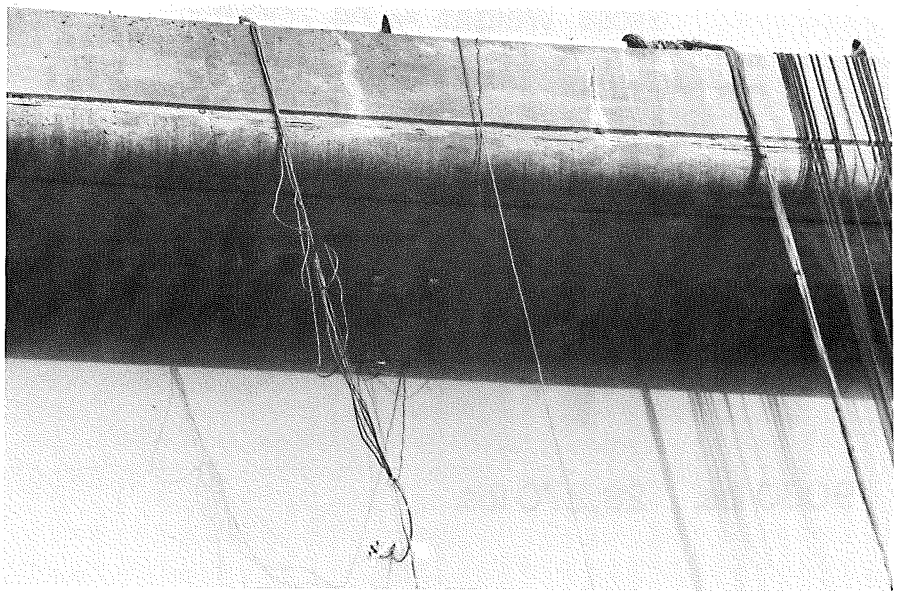

Fig. 8 Strain Gages and Wiring, Girder G8 near Pier 7

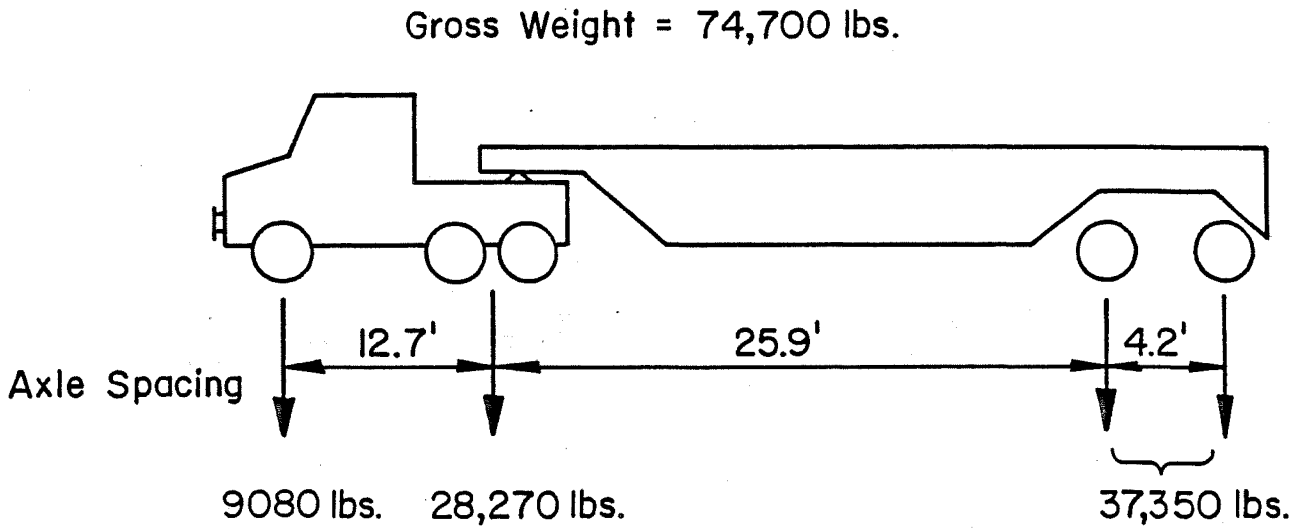

Fig. 9 Schematic of Test Truck

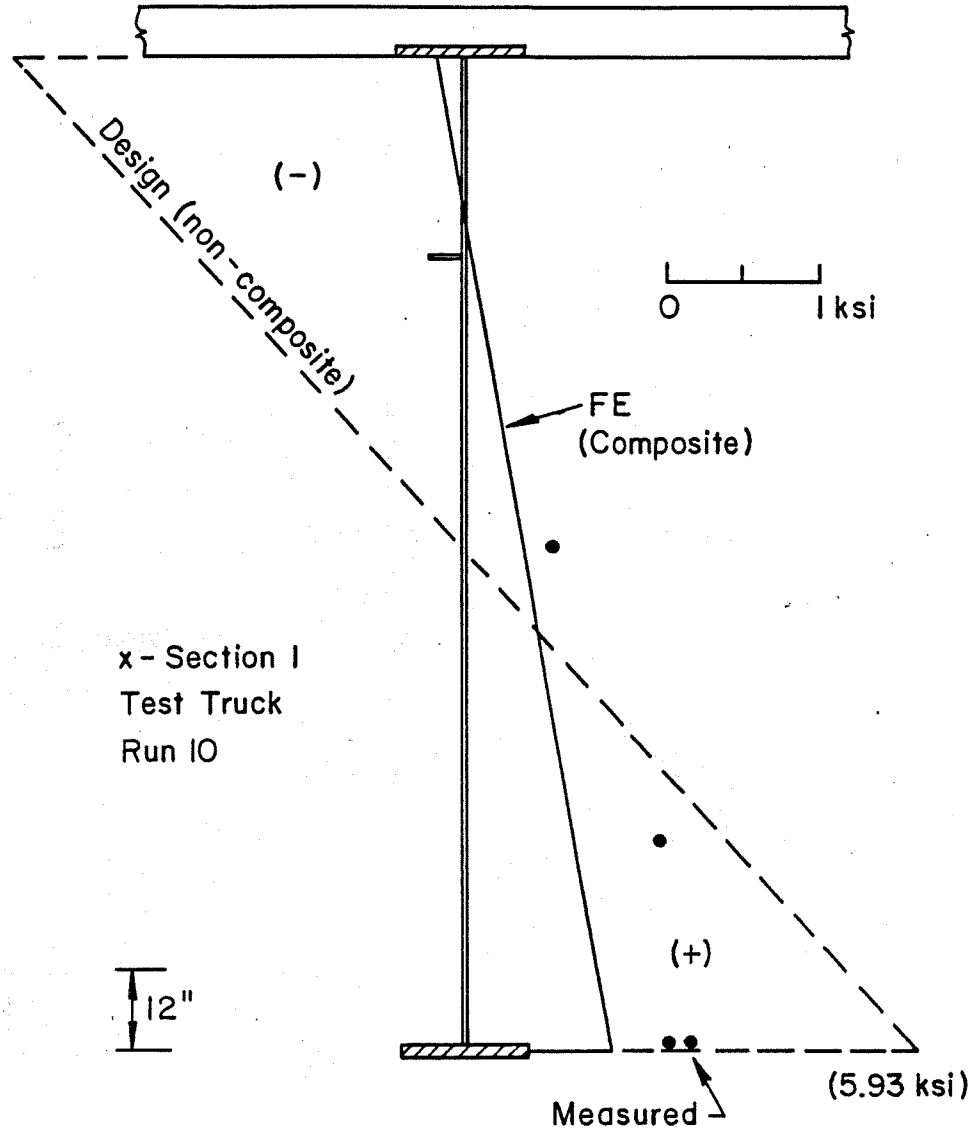

Fig. 10 Live Load Stresses at Cross Section 1

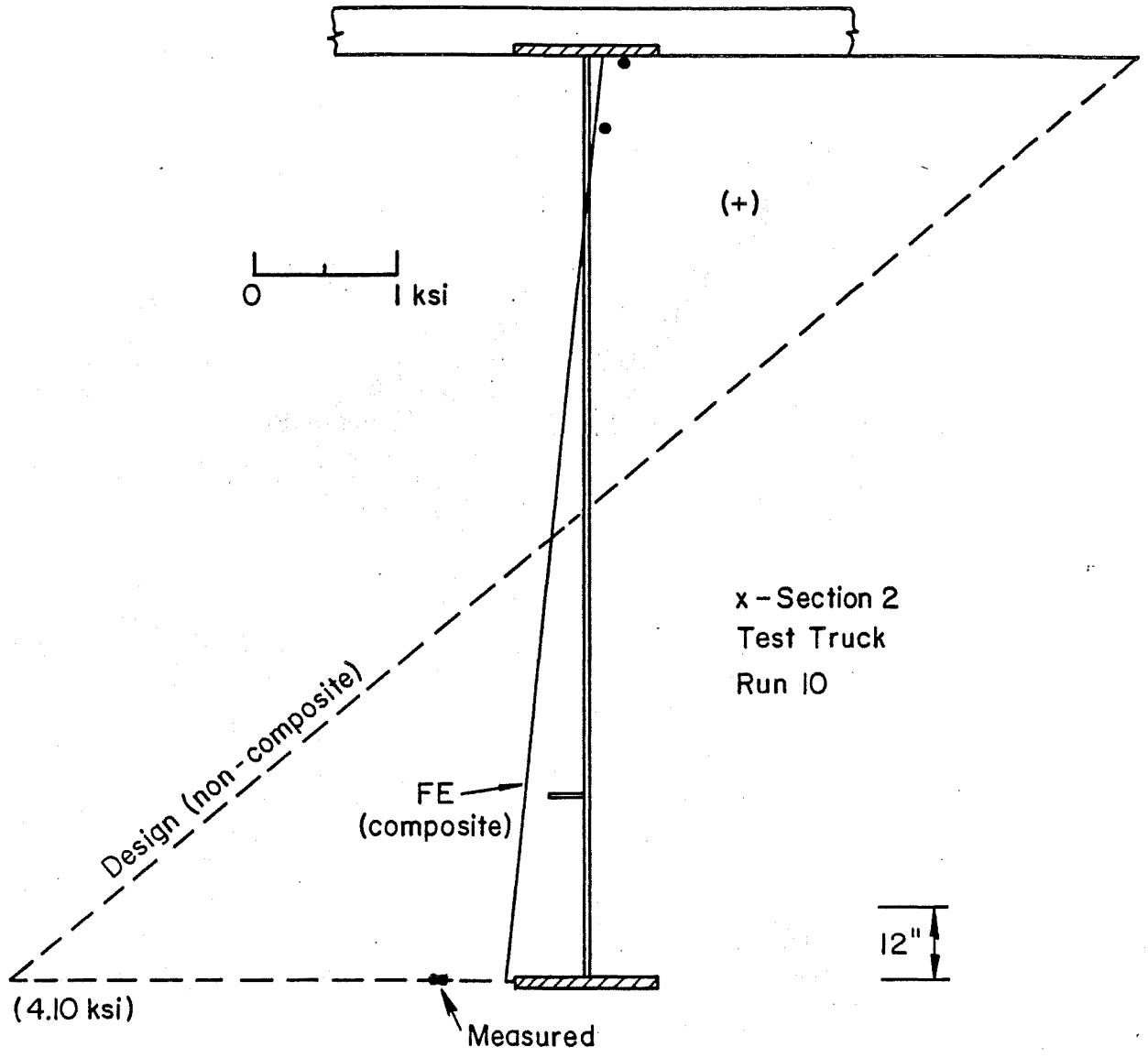

Fig. 11 Live Load Stresses at Cross Section 2

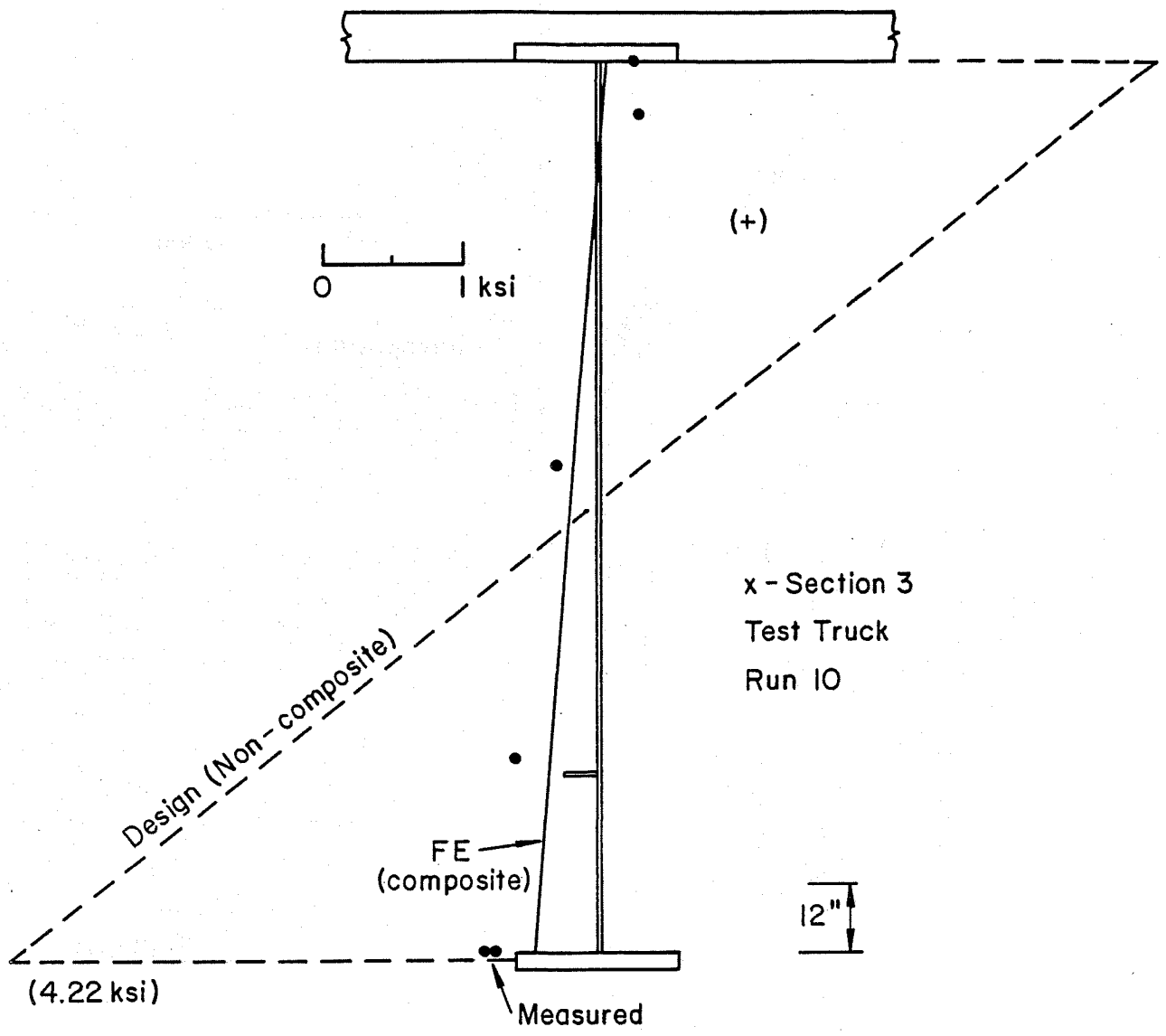

Fig. 12 Live Load Stresses at Cross-Section 3

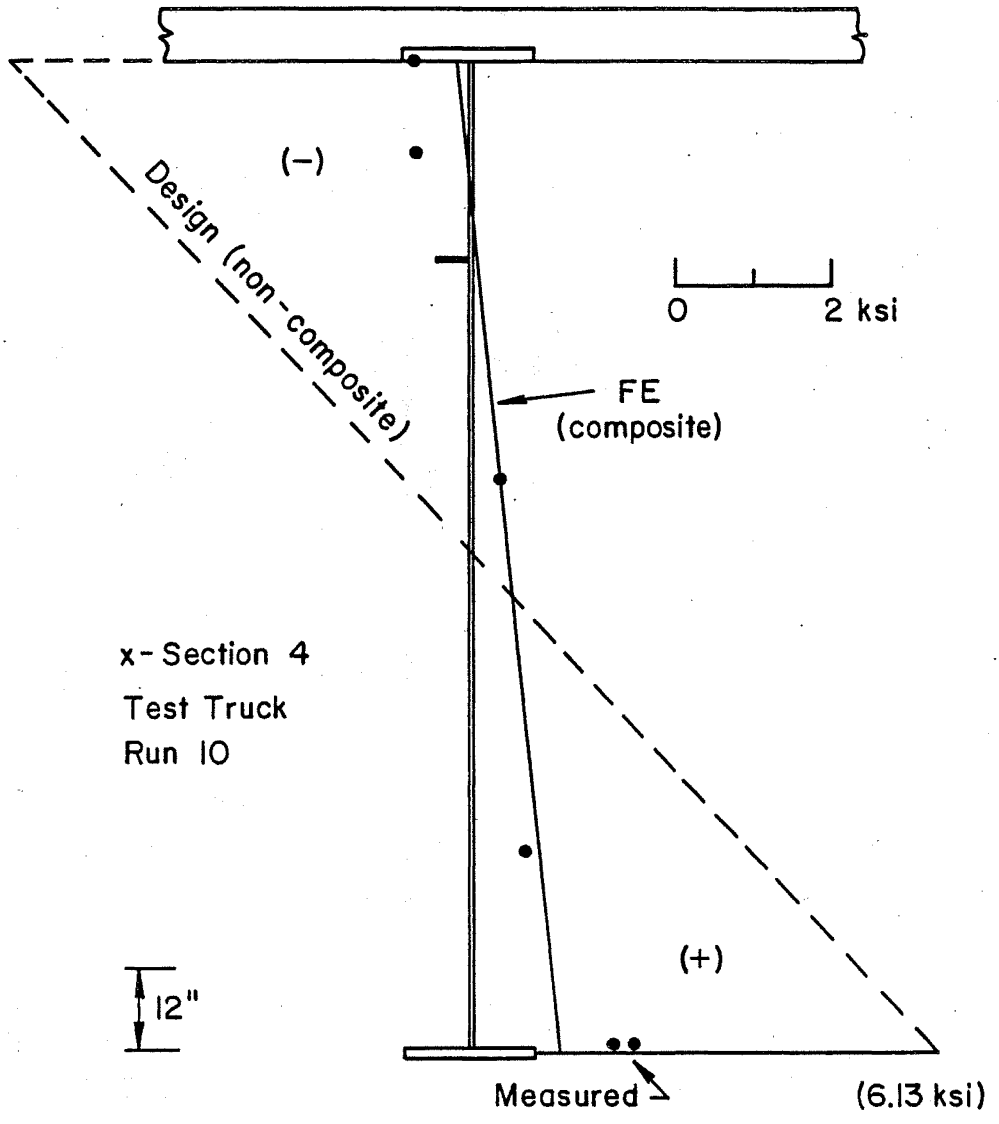

Fig. 13 Live Load Stresses at Cross-Section 4

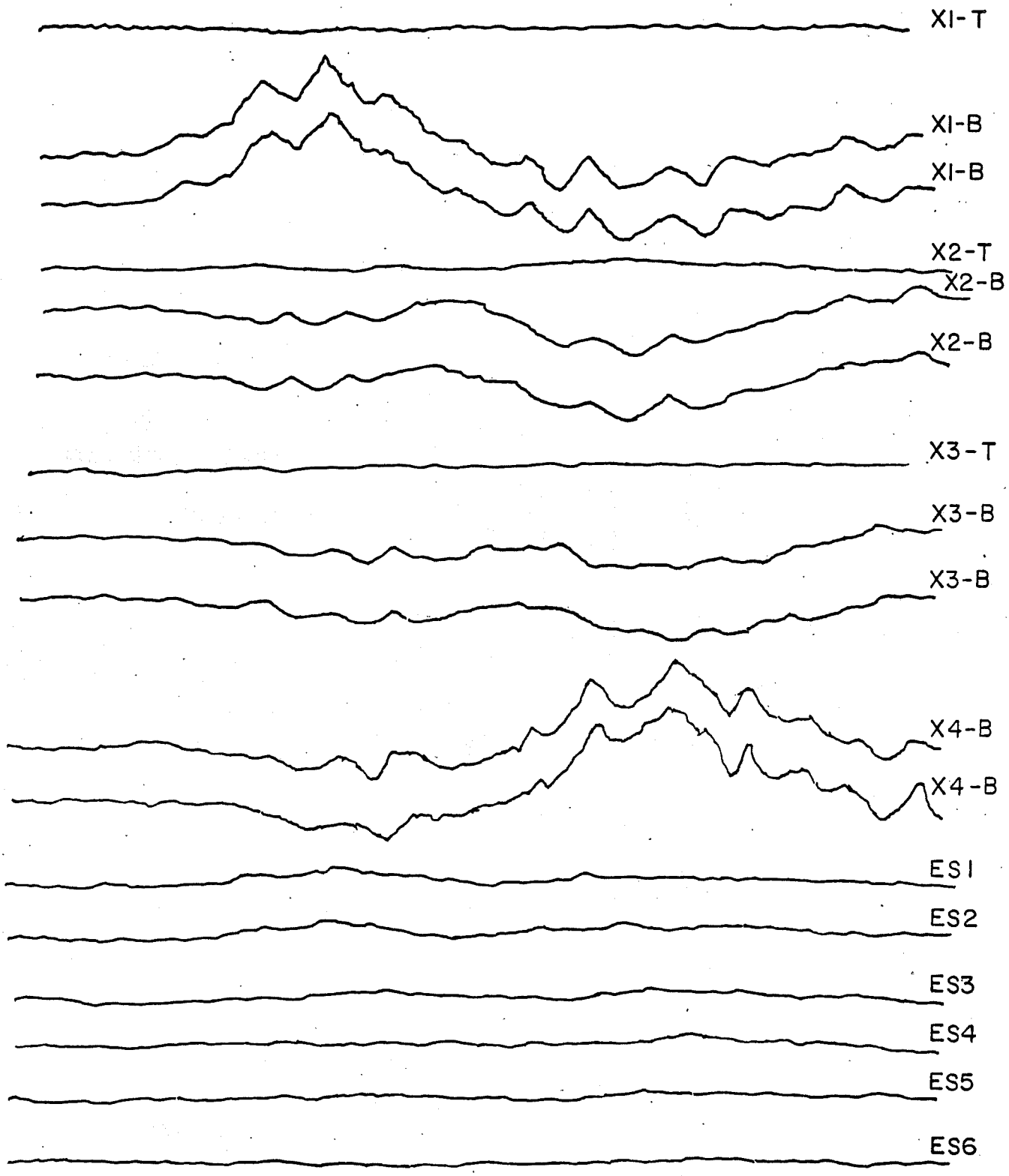

Fig. 14 Traces of Strain vs. Time Records from UV Recorders

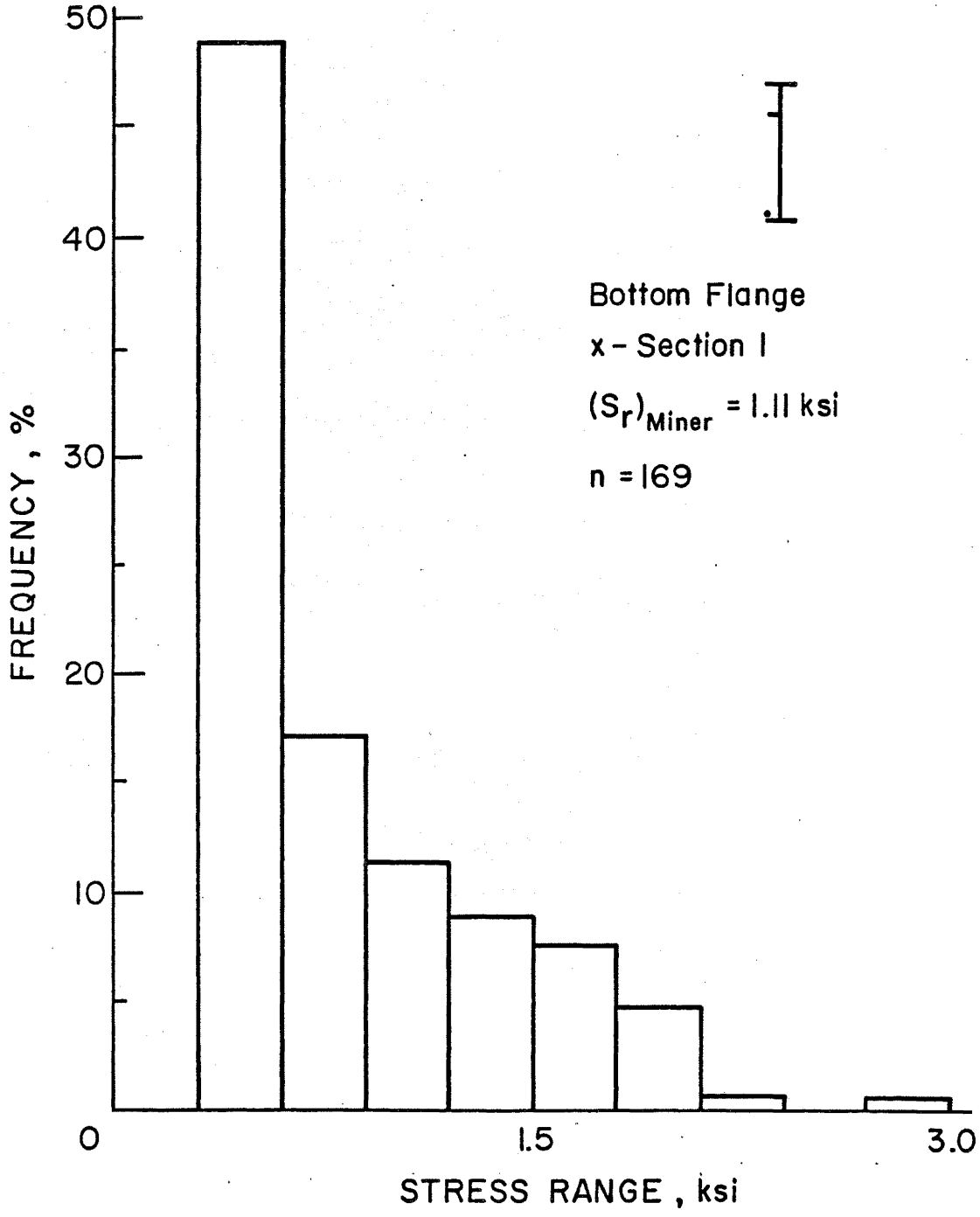

Fig. 15 Stress Range Histogram for Bottom Tension Flange of Span 7 at Cross-Section 1

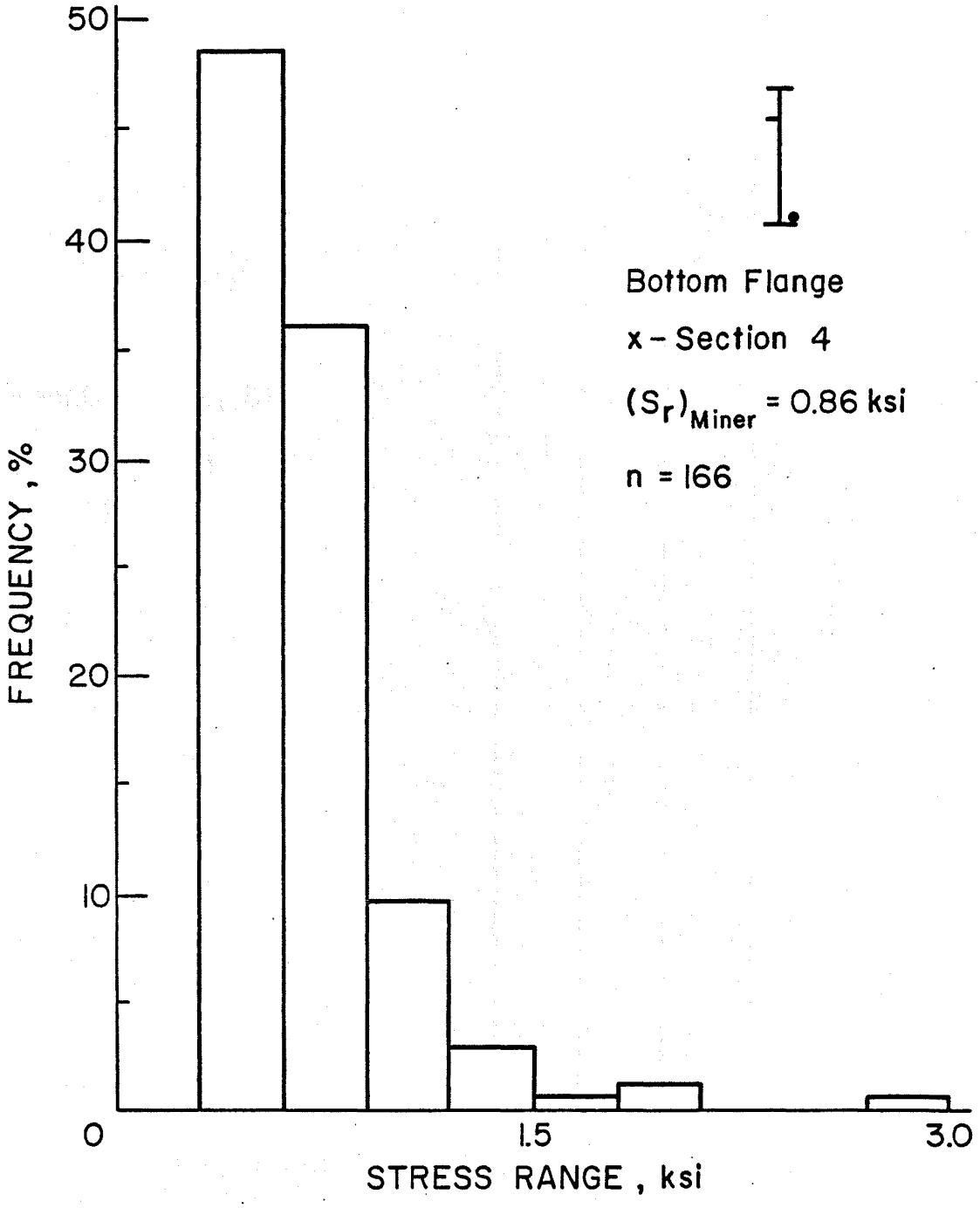

Fig. 16 Stress Range Histogram for Bottom Tension Flange of Span 8 at Cross-Section 4

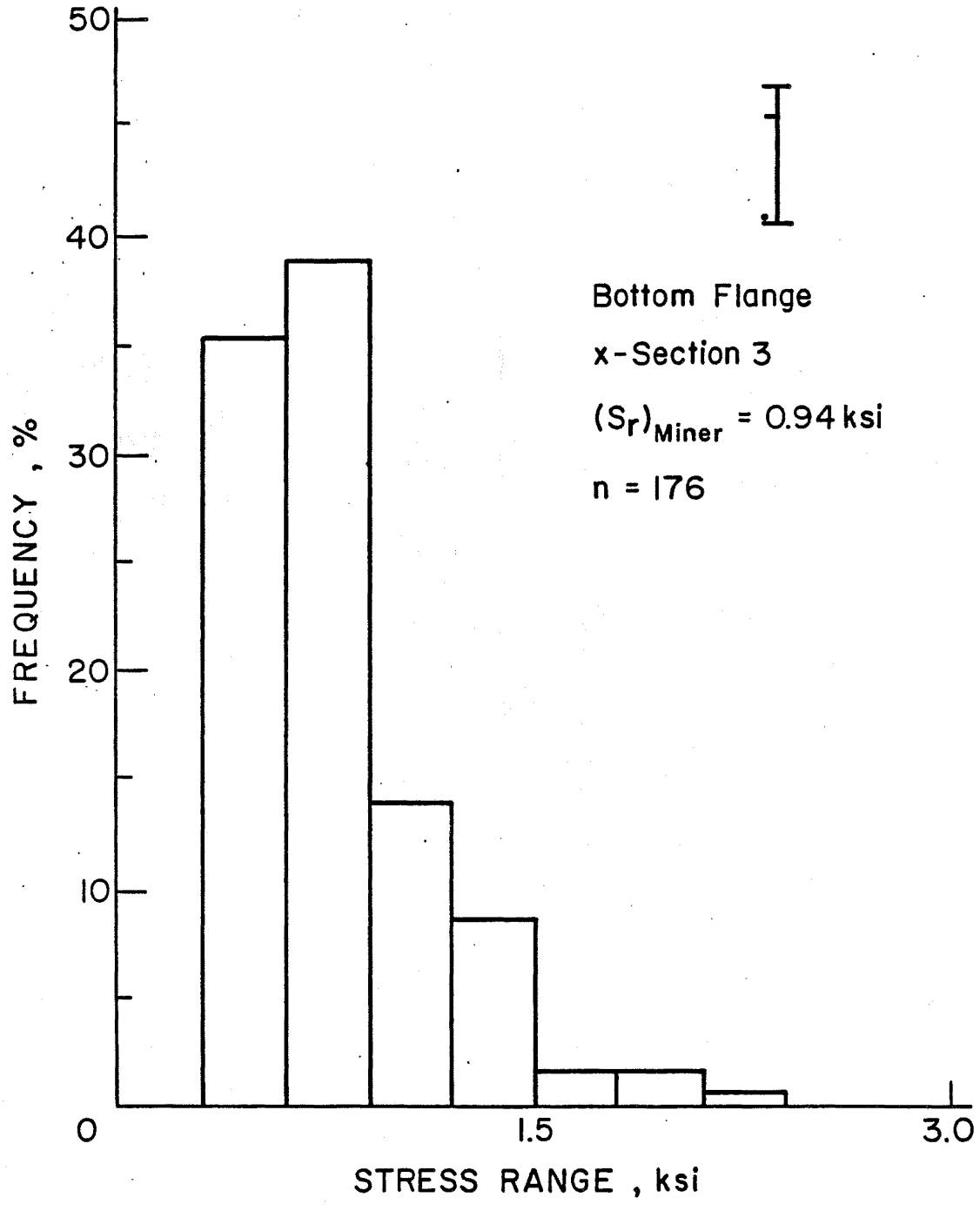

Fig. 17 Stress Range Histogram for Bottom Compression Flange of Span 8 at Cross-Section 3

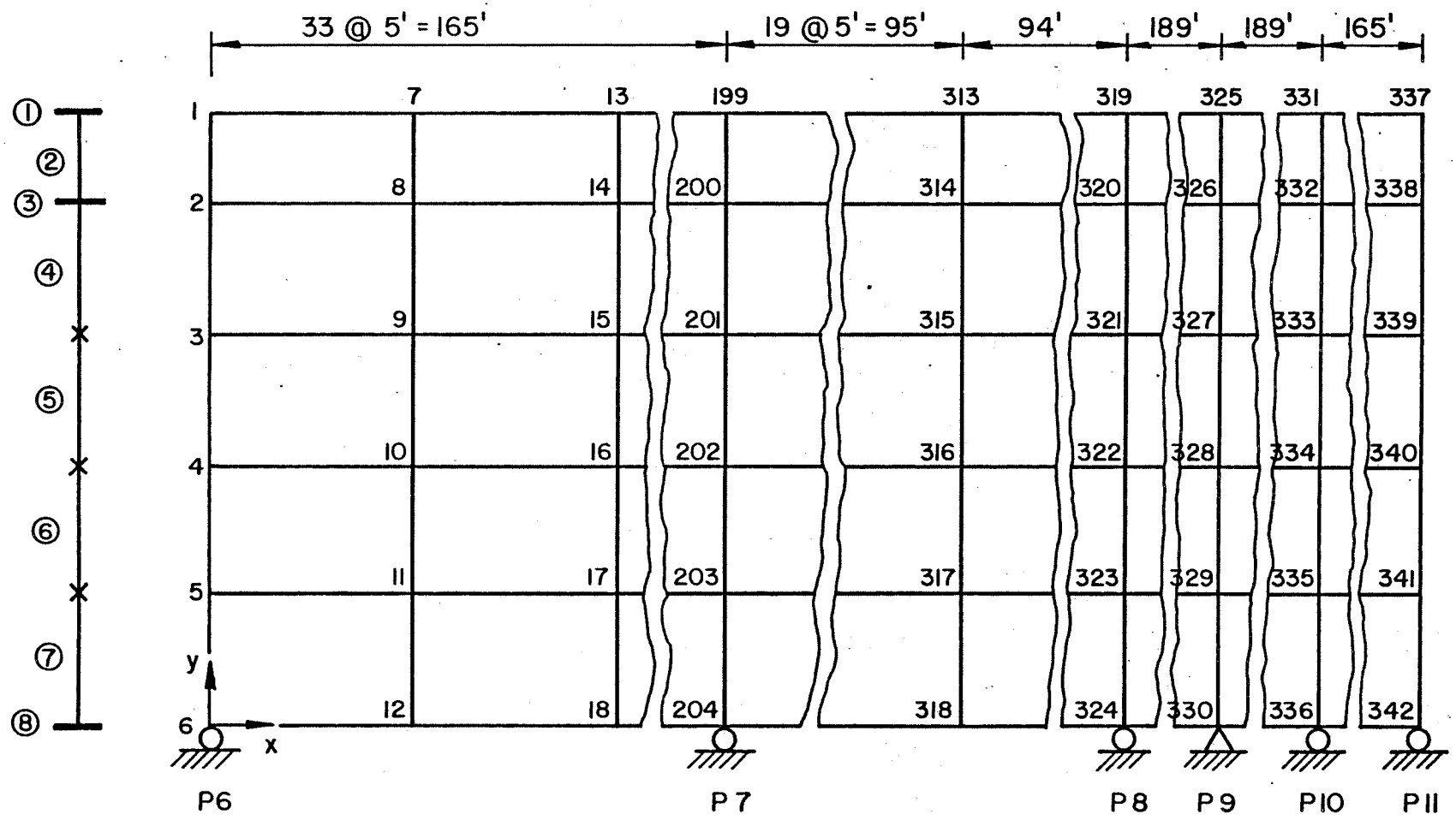

Fig. 18 Finite Element Model

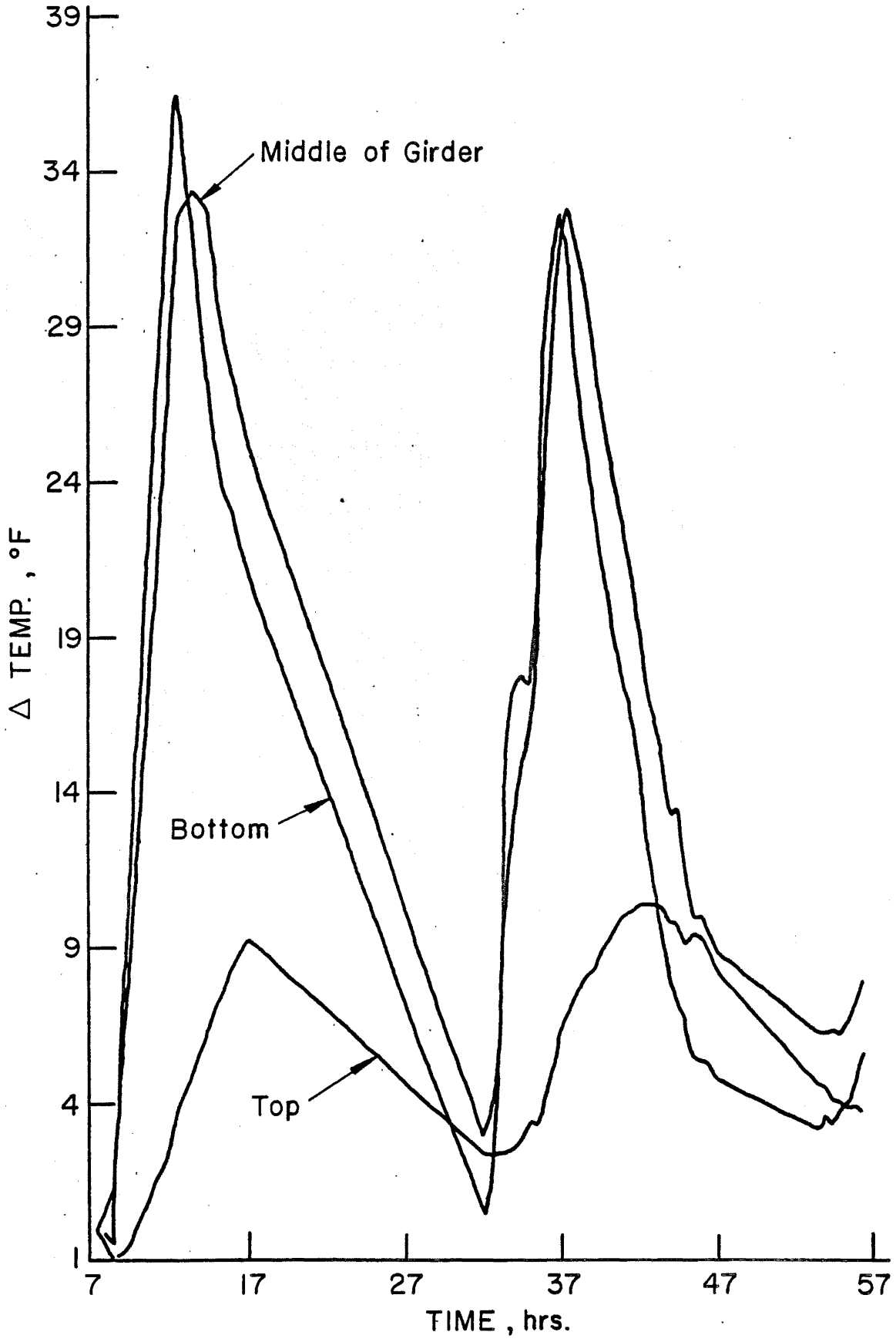

Fig. 19 Temperature vs. Time Cross-Section 1

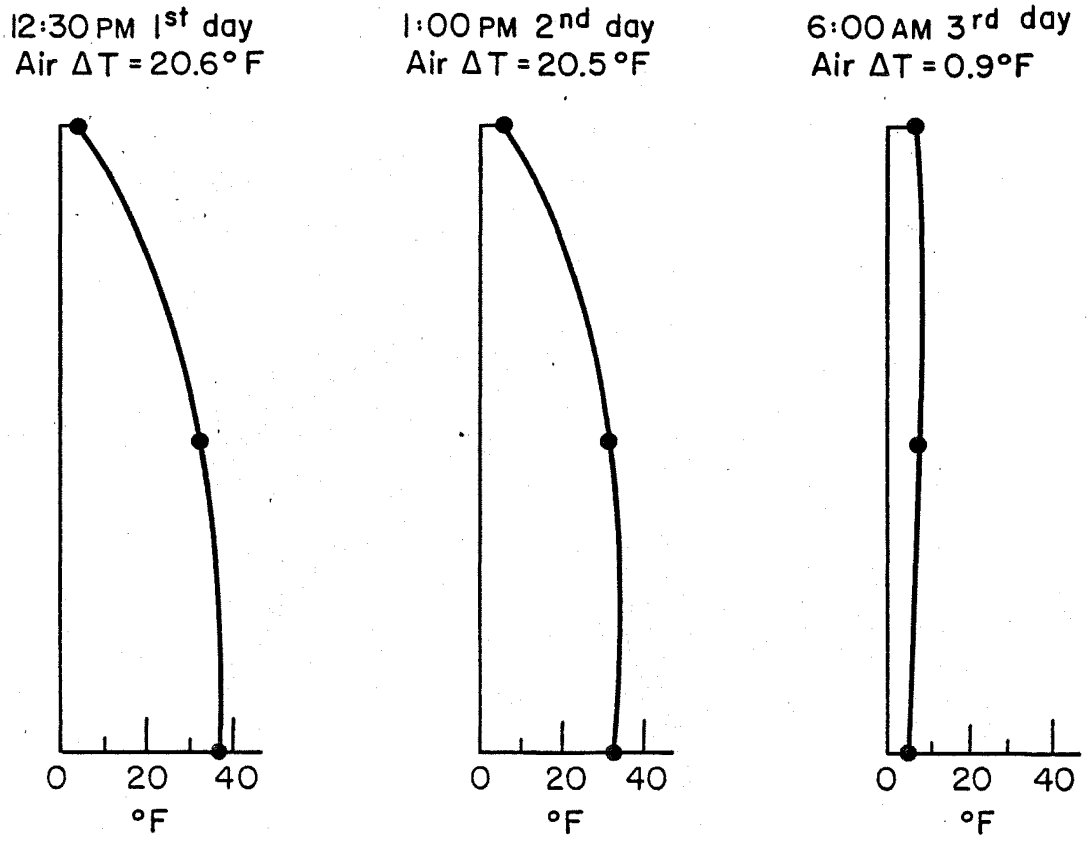

Fig. 20 Temperature Differential Across Cross-Section 1

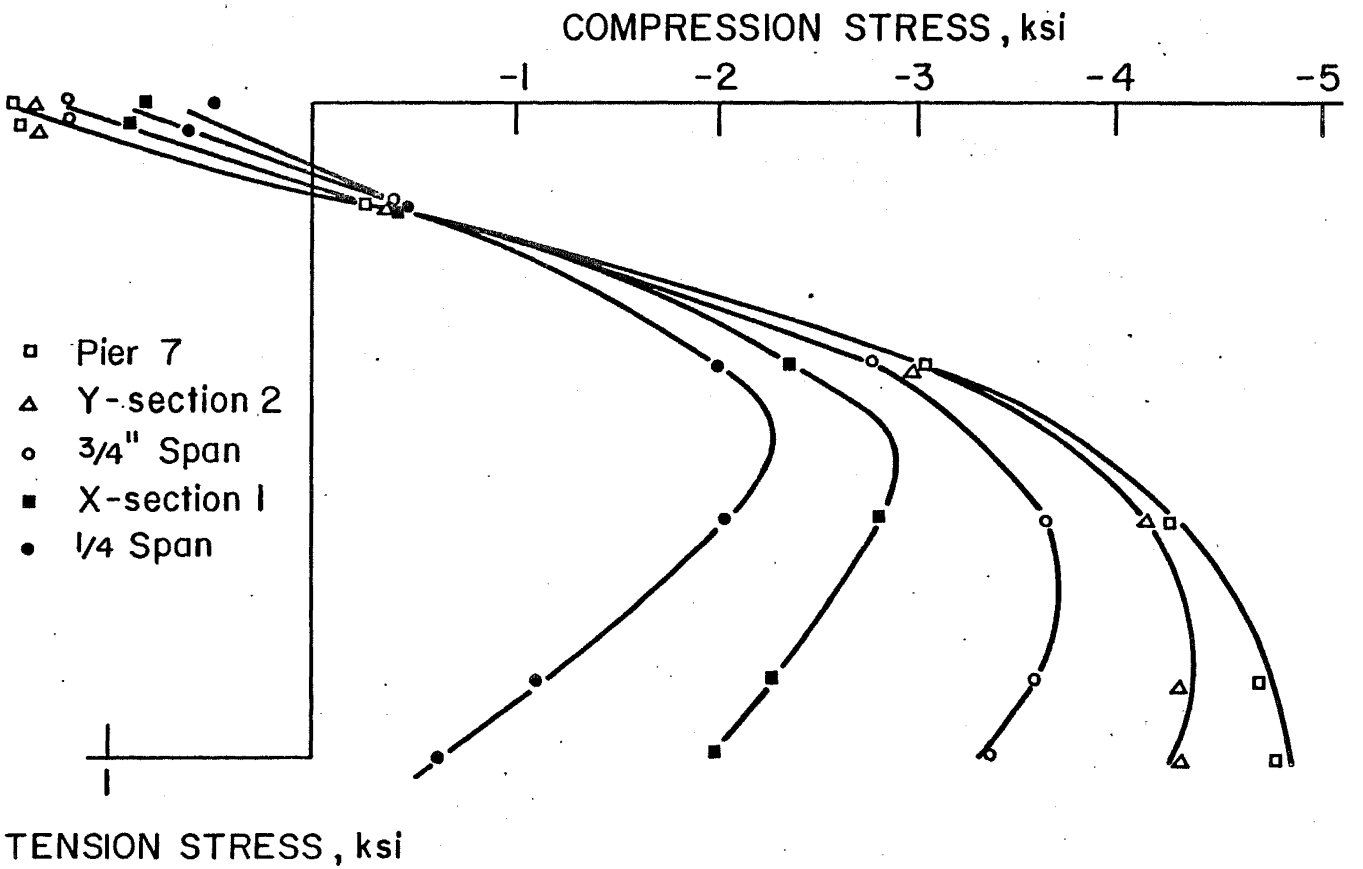

Fig. 21 "Hot Day" Thermal Stress Distribution (Span 7)

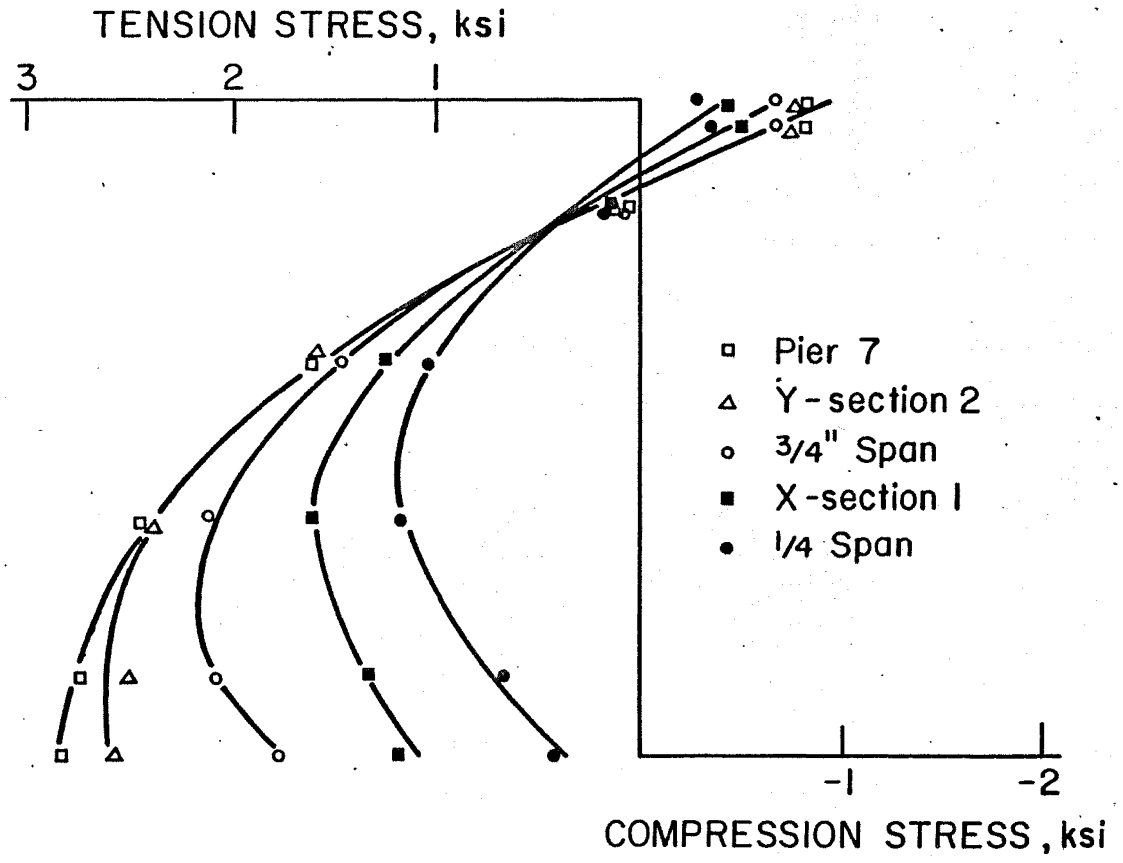

Fig. 22 "Cold Night" Thermal Stress Distribution (Span 7)

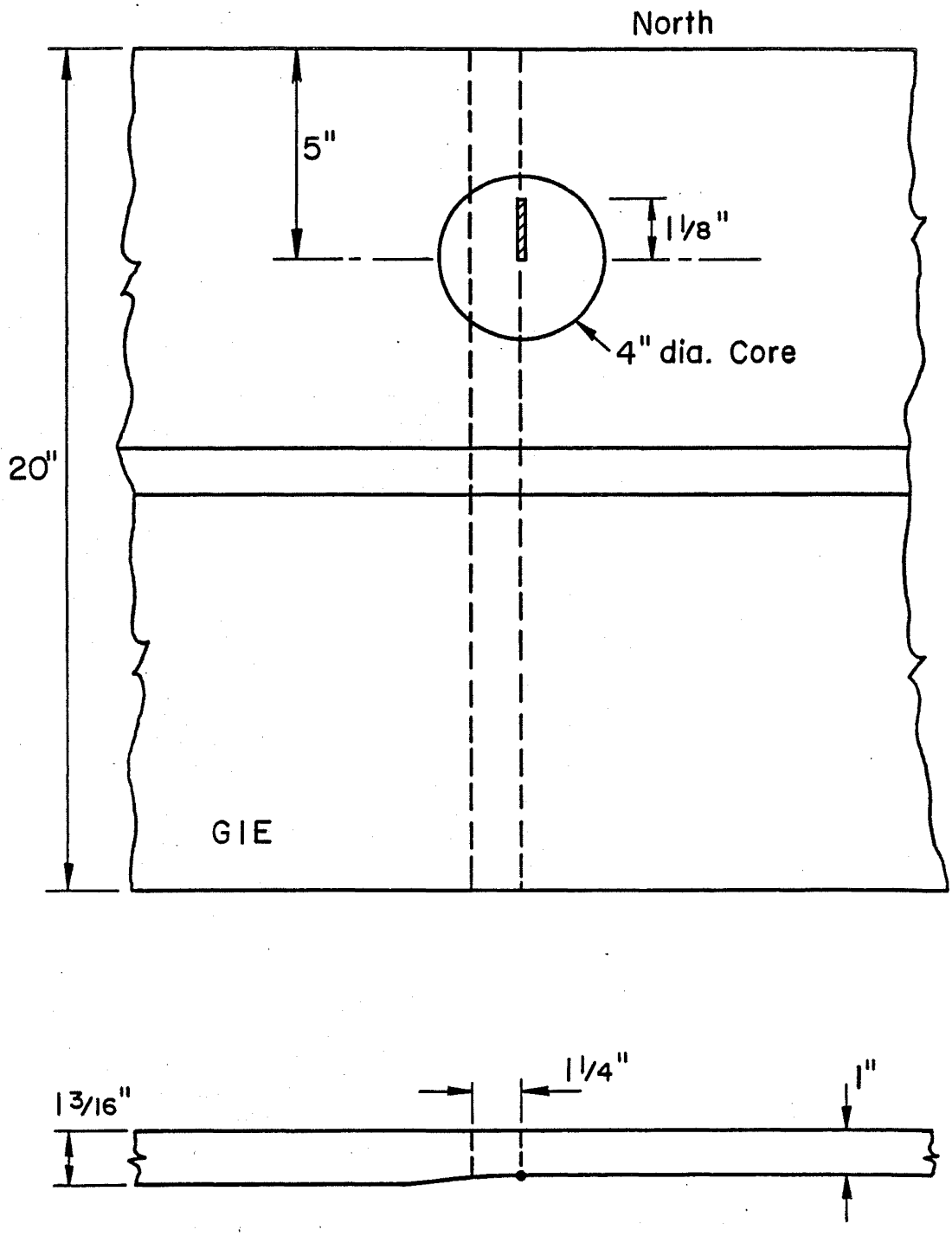

Fig. 23 Location of Defect in Electroslag Weldment G1E by Nondestructive Testing

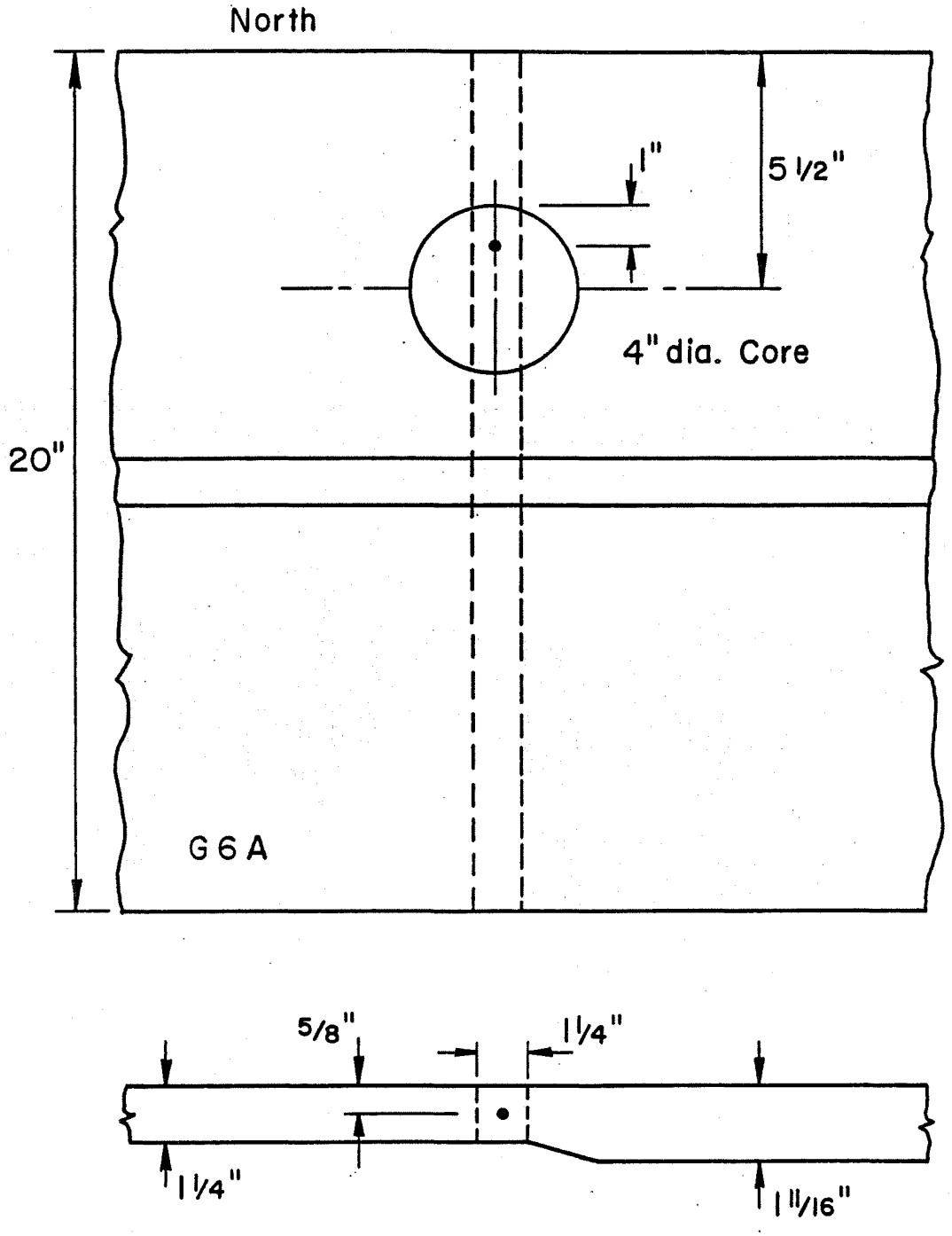

Fig. 24 Location of Defects in Electroslag Weldment G6A by Nondestructive Testing

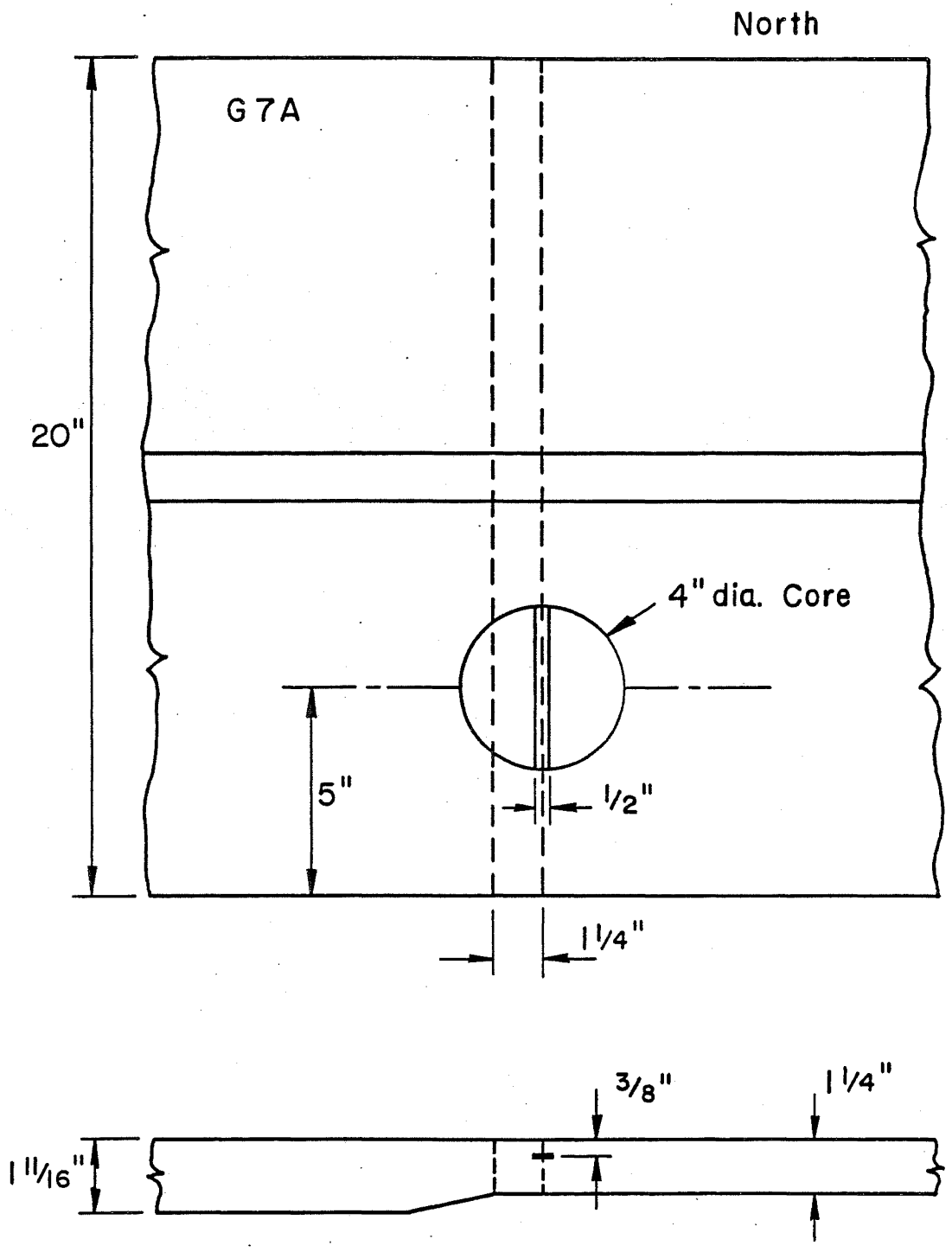

Fig. 25 Location of Defect in Multipass Weldment G7A by Nondestructive Testing

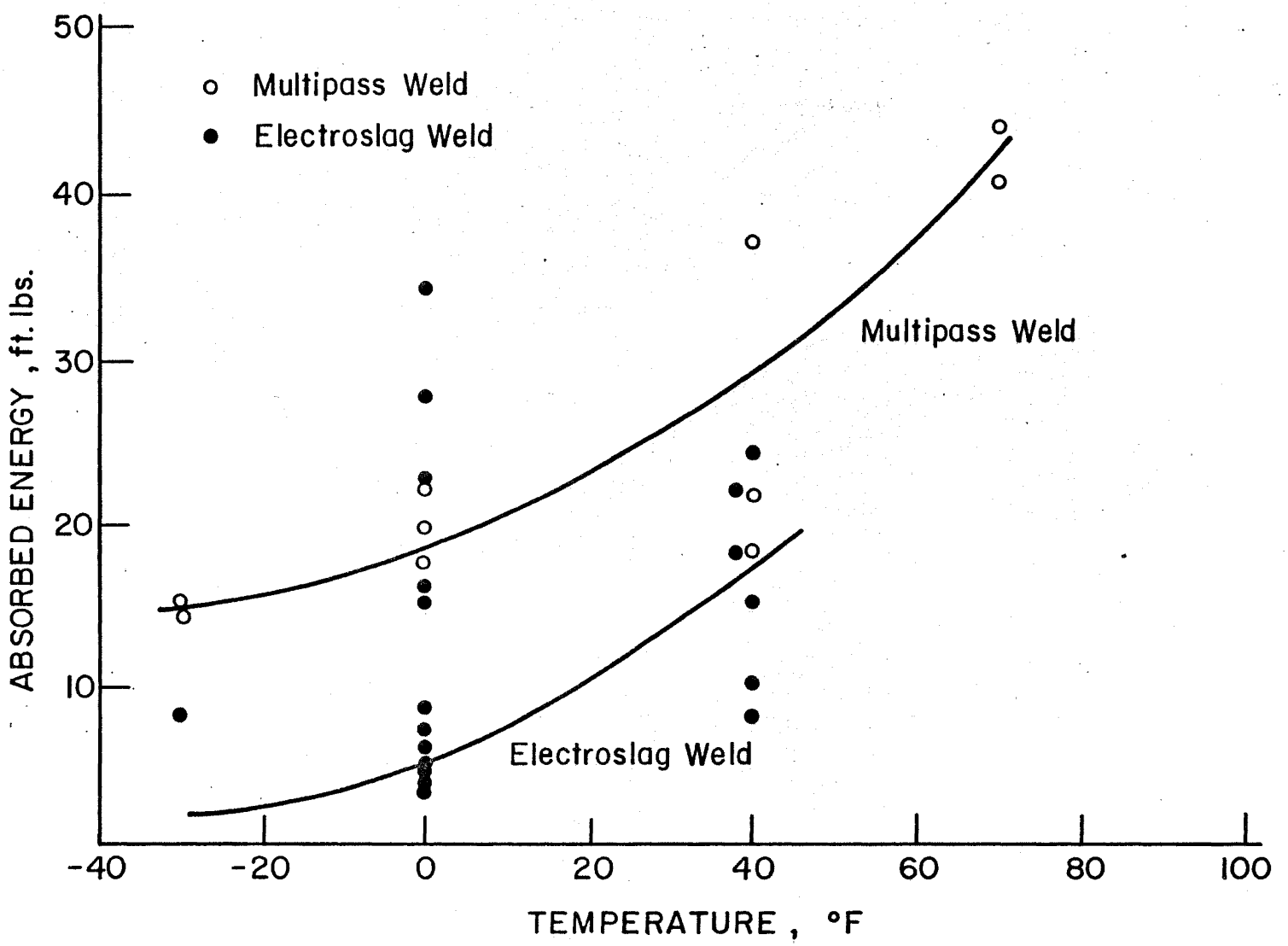

Fig. 26 CVN Absorbed Energy vs. Temperature

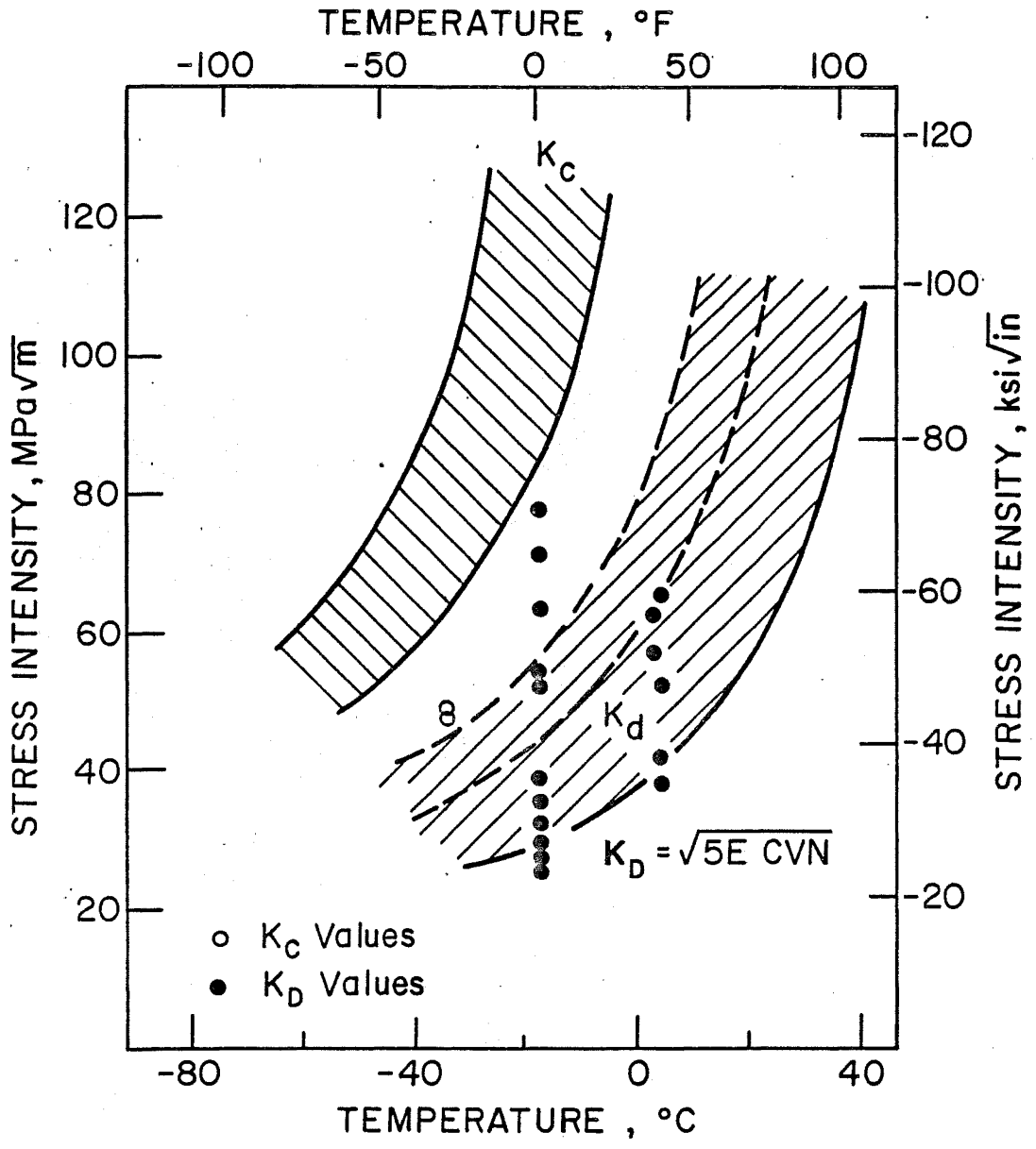

Fig. 27 Comparison of Fracture Toughness Estimates from Charpy V-Notch Data with Available K Data from Electroslag Welds

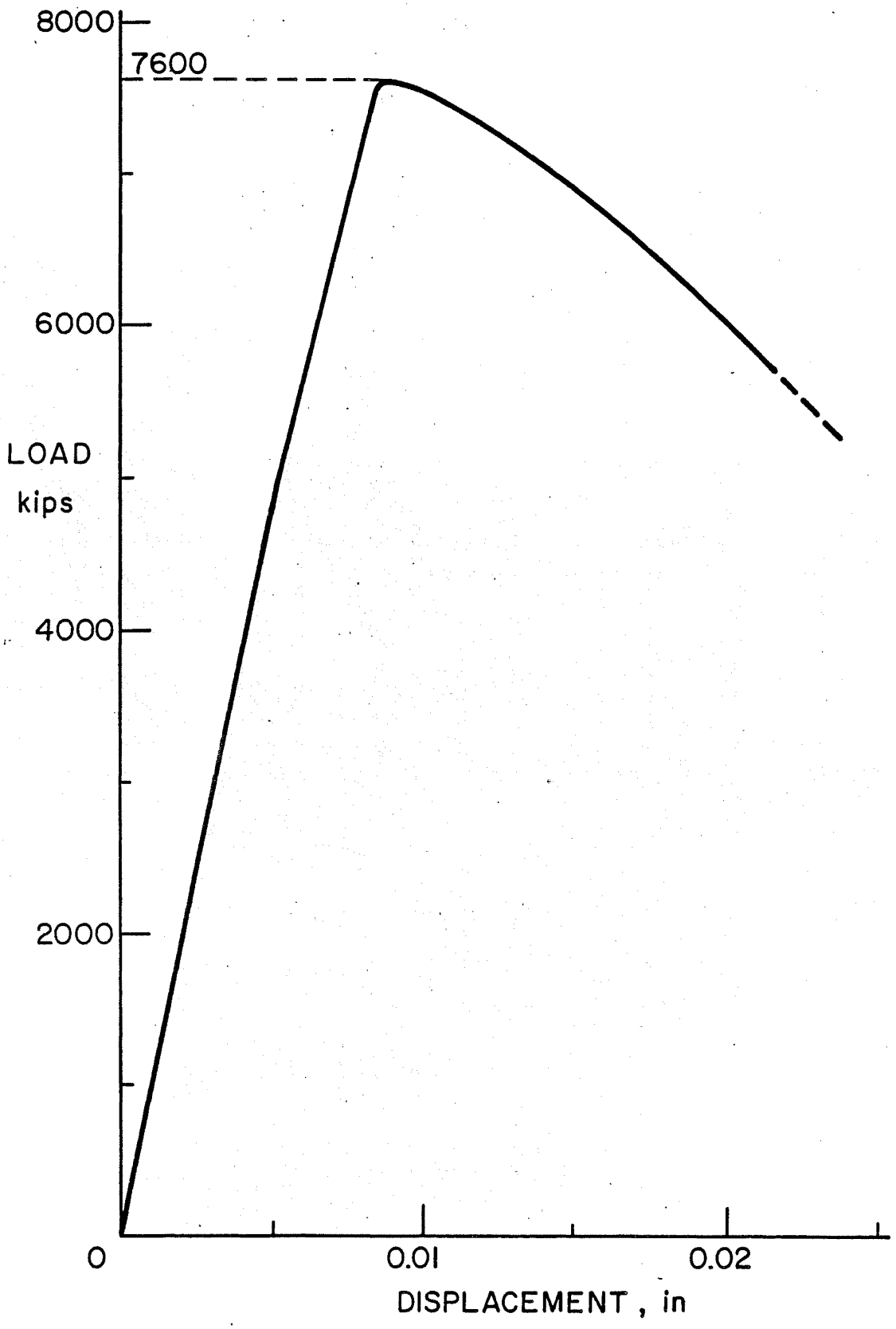

Fig. 28 Load-Deflection Curve for Compact Tension Specimen G6A

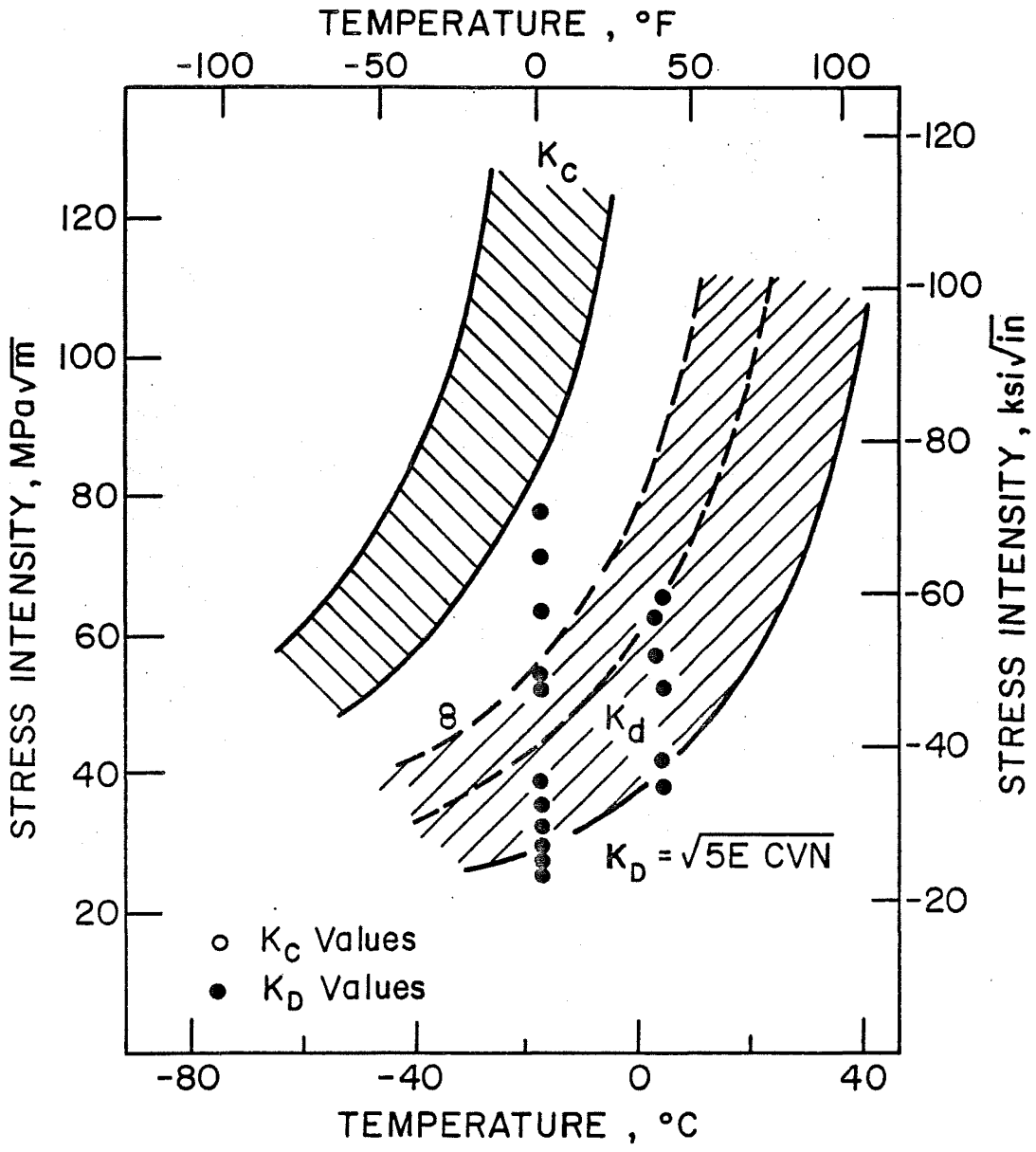

Fig. 29 Comparison of Fracture Toughness Estimates from Charpy V-Notch Data on Submerged Arc Weld G7A with Electroslag Weld Data

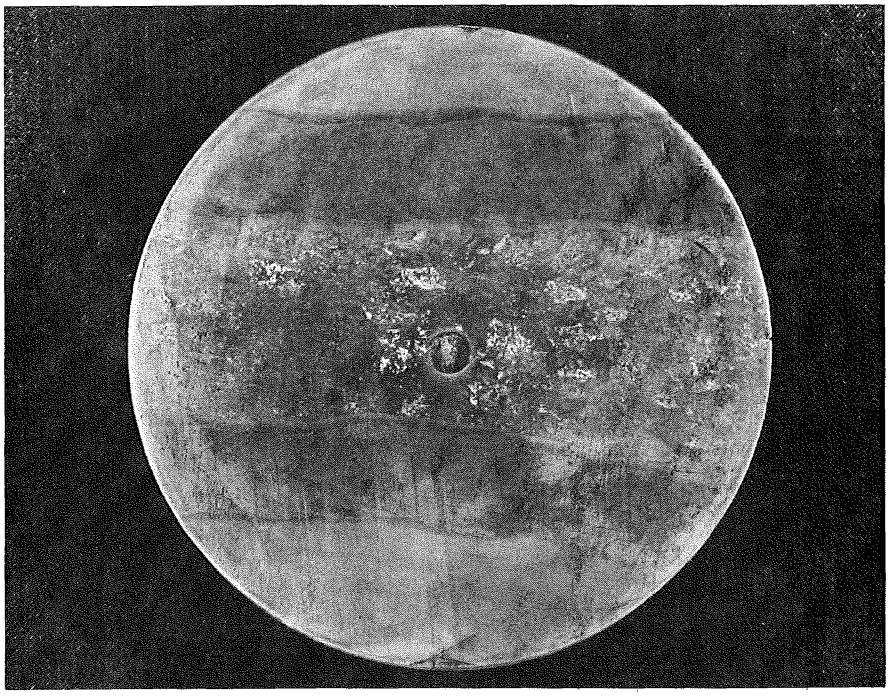

Fig. 30 Polished and Etched Surface of Core G1E

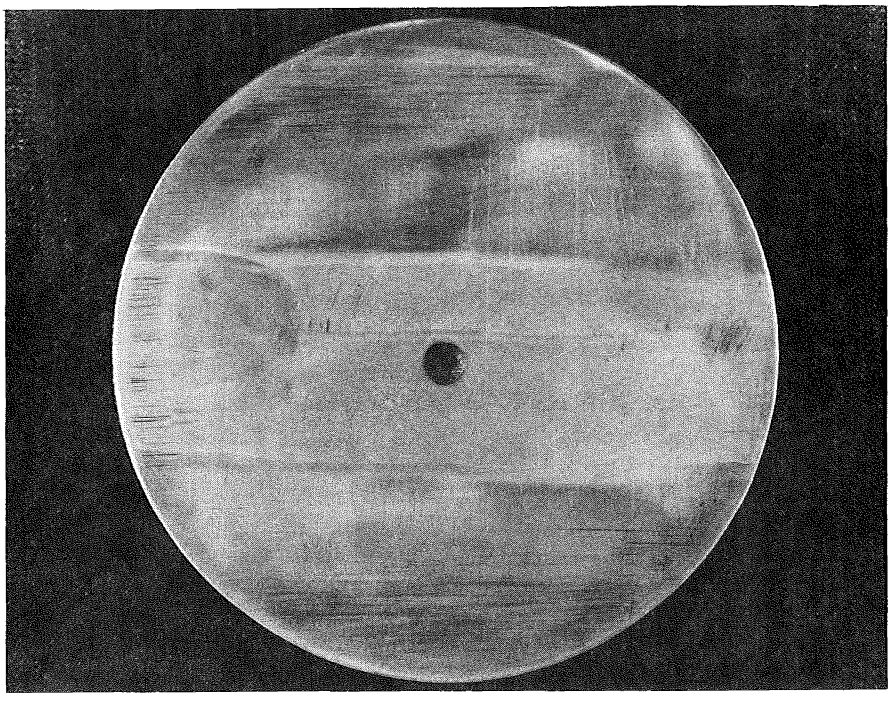

Fig. 31 Polished and Etched Surface of Core G7A

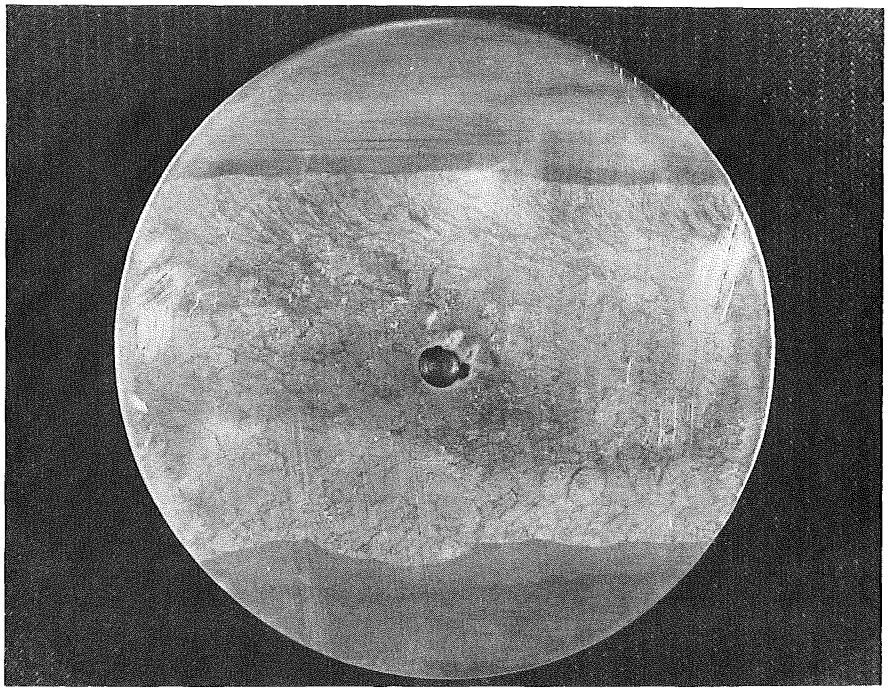

Fig. 32 Polished and Etched Surface of Core G6A

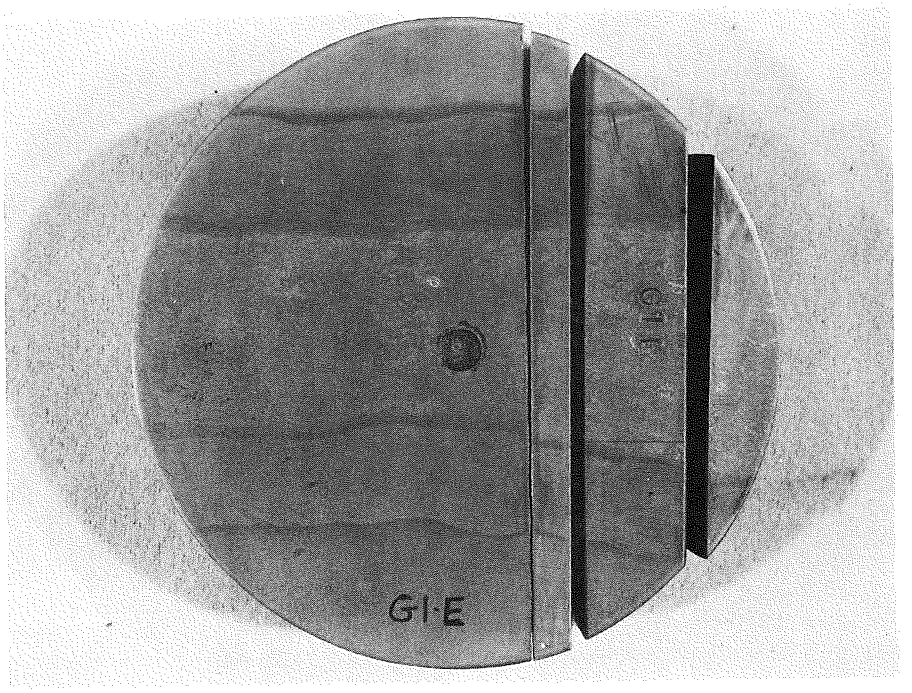

Fig. 33 Core G1E Cut into Segments for Destructive Examination

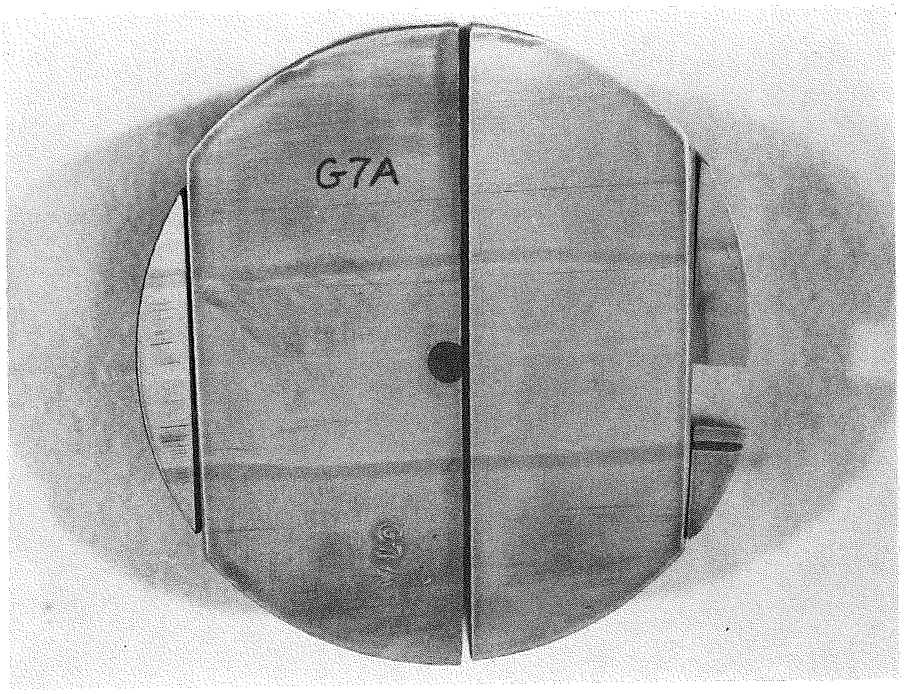

Fig. 34 Core G7A Cut into Segments for Destructive Examination

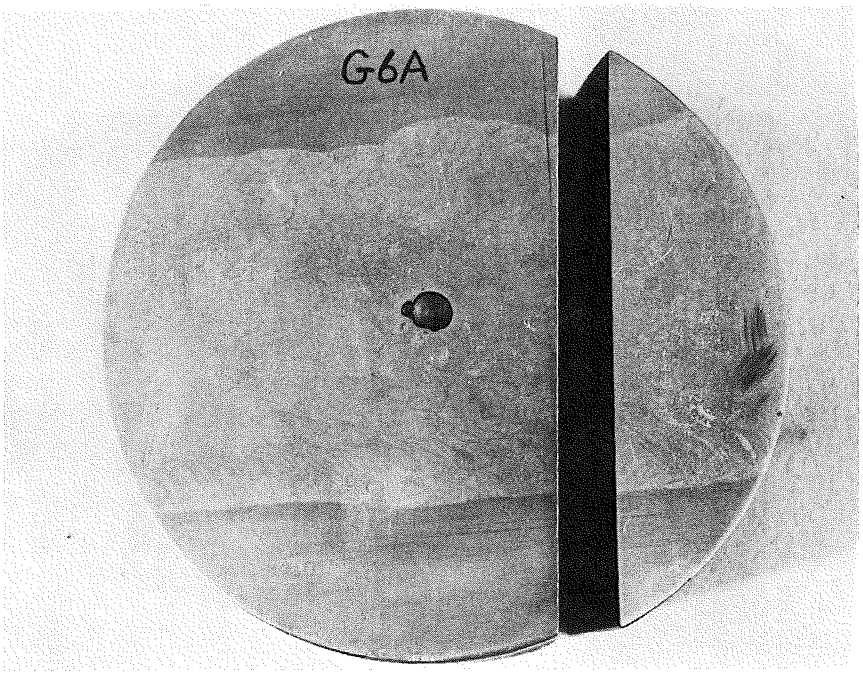

Fig. 35 Core G6A Cut into Segments for Destructive Examination

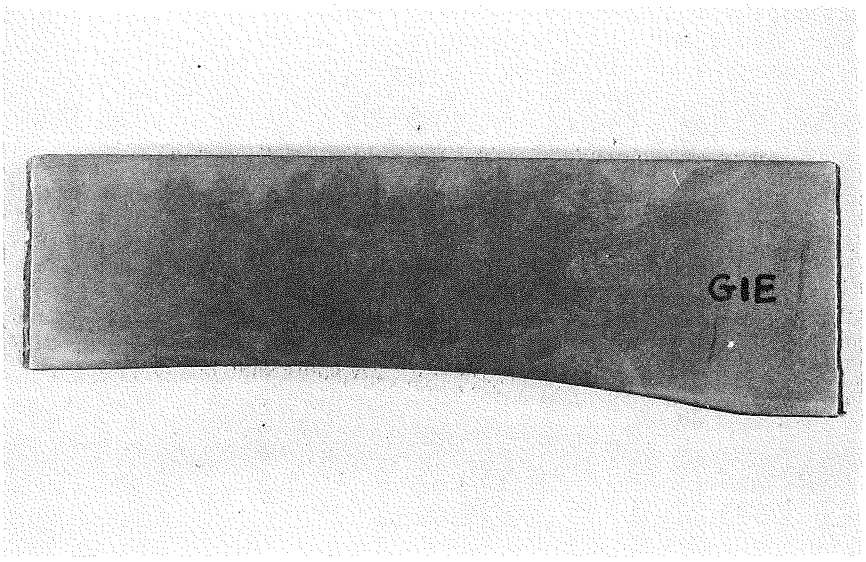

Fig. 36 Polished and Etched Surface G1E

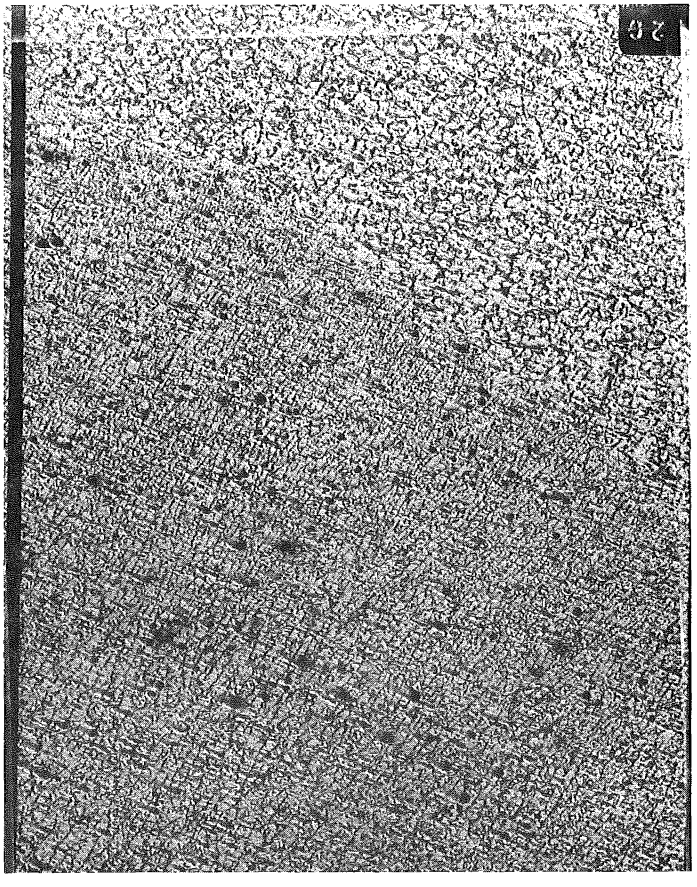

Fig. 37 Photomicrograph at 50X G1E

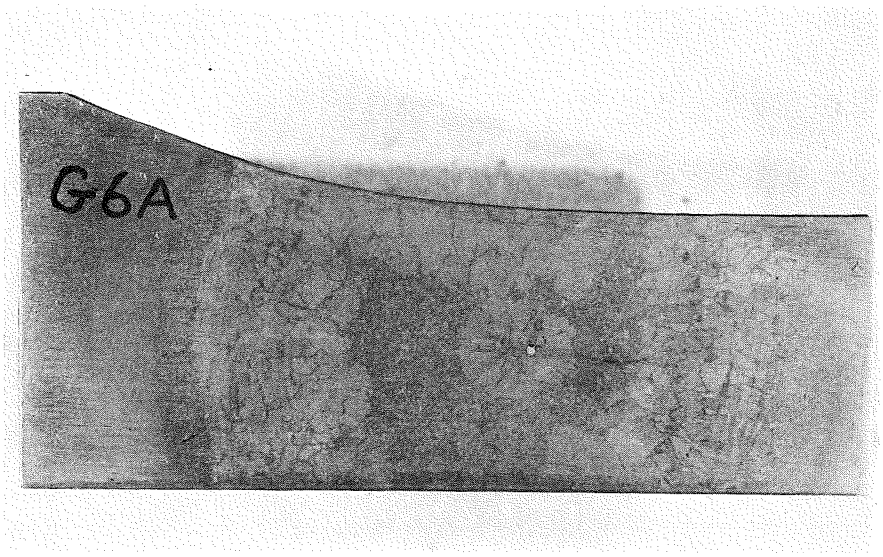

Fig. 38 Polished and Etched Surface G6A

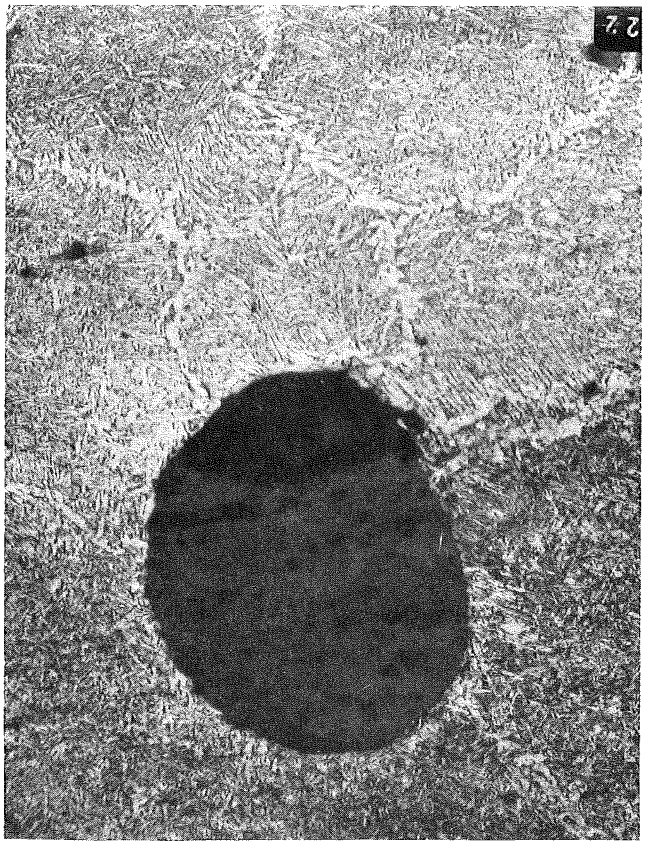

Fig. 39 Photomicrographs at 40X G6A

Fig. 40 Polished and Etched Surface G7A

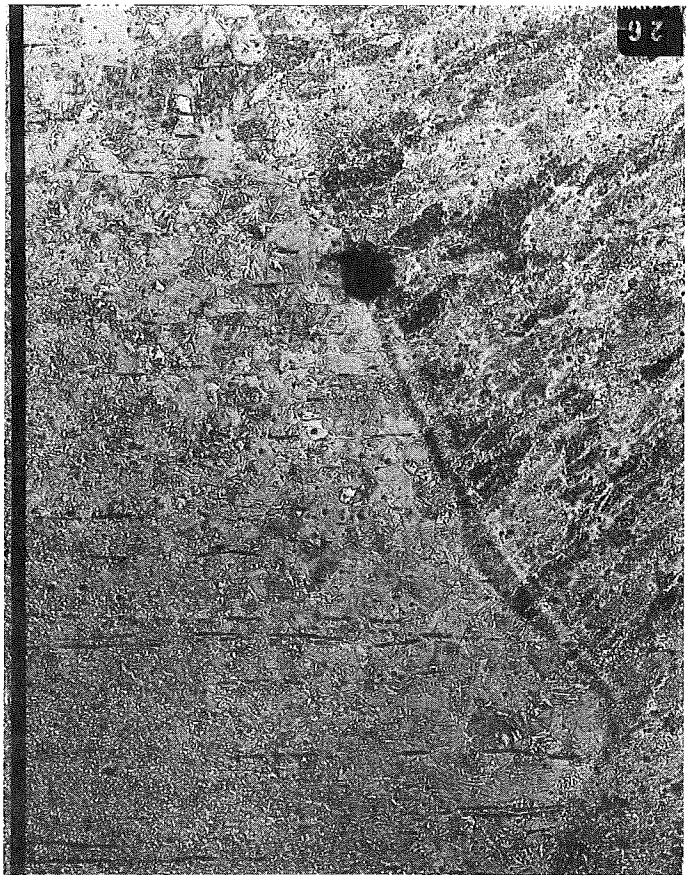

Fig. 41 Photomicrographs at 50X G7A

REFERENCES

1. Fisher, J. W., Pense, A. W., Wood, J. D. and Somers, B. R.
AN EVALUATION OF ELECTROSLAG WELDS IN THREE BRIDGES, Fritz Engineering Laboratory Report 438-1(81), March 1981

2. Ostapenko, A.
RIO-NITEROI BRIDGE: THERMAL FIELD STUDIES, Transportation Research Record 607, Transportation Research Board, 1977

3. Emmanuel, J. H. and Hulsey, L.
TEMPERATURE DISTRIBUTION IN COMPOSITE BRIDGES, Journal of the Structural Division, ASCE, Vol 104, No ST1, January 1978

4. Benter, W. P. and Schilling, C. G.
ACCEPTANCE CRITERIA FOR ELECTROSLAG WELDMENTS IN BRIDGES, NCHRP Report 201, Transportation Research Board, May 1979

5. Culp, J. D.
ELECTROSLAG WELDMENTS - PERFORMANCE AND NEEDED RESEARCH, Welding Journal, Vol 58, No 7, July 1979, pp 27-41

ACKNOWLEDGMENTS

The study reported herein was part of the Fritz Engineering Laboratory Project 457, sponsored by the Pennsylvania Department of Transportation and the Federal Highway Administration. The project was conducted at the Fritz Engineering Laboratory and Whitaker Laboratory, Lehigh University, Bethlehem, Pennsylvania.

The authors wish to thank Mr. Ronald Flegel of Pennsylvania Department of Transportation and his co-workers for their assistance during the field work. Mr. Harry Laatz of Federal Highway Administration, U. S. Department of Transportation, assisted with collecting strain and temperature data using FHWA equipment.

Appreciation is due Ms. Shirley Matlock and Mrs. Ruth Grimes for typing the manuscript, Mr. John Gera for tracing the figures, Mr. Richard Sopko for the photographic work, and Mr. Hugh Sutherland for the field instrumentation.